1 **Regulation of late-acting operons by three transcription factors and a CRISPR-Cas component**

2 **during *Myxococcus xanthus* development**

3 **Shreya Saha and Lee Kroos***

4 *Department of Biochemistry and Molecular Biology*, *Michigan State University*, *East Lansing*, *MI*

5 *48824*, *USA.*

6 Running title: Complex regulation of sporulation genes during *M. xanthus* development

7 *For correspondence. E-mail kroos@msu.edu; Tel. (+1) 517 355 9726; Fax (+1) 517 353 9334.

8

Summary

Upon starvation rod-shaped *Myxococcus xanthus* bacteria form mounds and then differentiate into round stress-resistant spores. Little is known about the regulation of late-acting operons important for spore formation. C-signaling has been proposed to activate FruA, which binds DNA cooperatively with MrpC to increase transcription of many genes. We report that this model can explain regulation of the *fadIJ* operon involved in spore metabolism, but not that of the spore coat biogenesis operons *exoA-I*, *exoL-P*, and *nfsA-H*. Rather, a mutation in *fruA* increased the transcript levels from these operons early in development, suggesting negative regulation by FruA initially, and a mutation in *mrpC* affected transcript levels from each operon differently. FruA bound to all four promoter regions *in vitro*, but strikingly each promoter region was unique in terms of whether or not MrpC and the DNA-binding domain of Nla6 bound, and in terms of cooperative binding. Furthermore, the DevI component of a CRISPR-Cas system is a negative regulator of all four operons, based on transcript measurements. Our results demonstrate complex regulation of sporulation genes by three transcription factors and a CRISPR-Cas component, which we propose thwarts viral intrusion while making spores suited to withstand starvation and environmental insults.

25 **Introduction**

26 The Gram-negative soil bacterium *Myxococcus xanthus* provides an attractive model system to
27 study signal-induced gene regulation and bacterial community behavior (1). Upon nutrient
28 depletion, cells move on solid surfaces and form mounds, within which some of the rod-shaped
29 cells differentiate into round, stress-resistant spores. During this multicellular developmental
30 process of fruiting body formation, a majority of the population undergoes lysis, while some
31 cells remain outside of fruiting bodies as peripheral rods (2, 3). Transcriptomic analyses
32 indicate that approximately 1500 (4, 5) to 4000 (6) genes (i.e., 20-50% of the genes) are up- or
33 down-regulated during *M. xanthus* development.

34 A signal-responsive gene regulatory network (GRN) governs the developmental process of
35 *M. xanthus* (7). Starvation triggers production of the intracellular secondary messenger
36 molecules (p)ppGpp (8, 9) and c-di-GMP (10), which lead to production of the extracellular A-
37 and C-signals (9, 11-14) and exopolysaccharide (10), respectively. Other signals are implicated
38 in the developmental process, but are less well-characterized in terms of their identity and/or
39 their impact on the GRN (15).

40 Among the better-characterized developmental signals of *M. xanthus*, early studies showed
41 that C-signal acts later than (p)ppGpp and A-signal (9, 11, 16, 17). The exchange of C-signal
42 between cells required their movement into alignment, possibly into contact (18-20). An
43 increasing level of C-signaling was proposed to ensure that cells first build mounds and then
44 form spores, resulting in multicellular fruiting bodies (21-23). The C-signal appears to be a
45 proteolytic fragment of the CsgA protein (24-26) and/or diacylglycerols produced by cardiolipin
46 phospholipase activity of full-length CsgA (27), but the mechanism(s) of signal transduction

47 remain to be elucidated. C-signaling appears to posttranslationally activate the transcription
48 factor FruA (28, 29) (Fig. 1), but the mechanism is unknown. FruA is similar to response
49 regulators of two-component signal-transduction systems (30). Response regulators are
50 typically activated by phosphorylation by a histidine kinase (28). However, for several reasons,
51 phosphorylation is unlikely to be the mechanism by which FruA is activated in response to C-
52 signaling (29, 31).

53 Transcription of the *fruA* gene is regulated by a cascade of starvation-responsive
54 transcription factors that includes MrpC (7, 32) (Fig. 1), which binds upstream of the *fruA*
55 promoter and stimulates transcription (33, 34). In addition to transcriptional control of the
56 *mrpC* gene by starvation (35), the level of MrpC protein is regulated by proteolysis (Fig. 1),
57 slowing the pace of development under the normal conditions of starvation (36, 37) and halting
58 development if sufficient nutrients are added back before rods become committed to spore
59 formation (38, 39). An N-terminally truncated form of MrpC called "MrpC2" was proposed to
60 be important for development (34), but recent work indicated that MrpC2 is likely an artifact of
61 the method of cell lysate preparation and that full-length MrpC is the active form *in vivo* (35), at
62 least in part due to a threonine/serine motif near its N-terminus (40). Both MrpC and MrpC2
63 bind to DNA *in vitro* (34, 35, 41).

64 *In vitro*, MrpC2 and FruA bind cooperatively to the promoter regions of many
65 developmentally-regulated genes (41). Mutational analyses of five such promoter regions (*dev*,
66 *fmgA*, *fmgBC*, *fmgD*, and *fmgE*) suggest that cooperative binding of MrpC and FruA to a site just
67 upstream of the promoter stimulates transcription *in vivo*, forming a feed-forward loop (Fig. 1,
68 only *dev* is shown), whereas binding to nearby sites can increase or decrease transcription (31,

69 42-45). The different arrangements of binding sites with different affinities for MrpC and FruA
70 may explain the observed differences between genes in terms of their spatiotemporal patterns
71 of expression and their extent of dependence on C-signaling for expression (7, 17, 46). The
72 levels of MrpC, FruA, and CsgA normally rise in starving rods engaged in mound building (3), but
73 the addition of sufficient nutrients triggers rapid proteolysis of MrpC and prevents the normal
74 increase in transcripts for proteins involved in sporulation (38, 39). Combinatorial control of
75 gene expression by MrpC and FruA appears to ensure that only starving rods (in which MrpC
76 and FruA are synthesized and stably accumulate) aligned in mounds (which enhances short-
77 range C-signaling between rods, presumably activating FruA within them) commit to spore
78 formation (7, 19, 31, 38, 46).

79 Among the genes combinatorially controlled by MrpC and FruA, early studies showed that
80 mutations in the *dev* operon can cause severe defects in sporulation (47-50). The *dev* operon
81 includes eight genes comprising a CRISPR-Cas system that has been proposed to protect
82 developing *M. xanthus* against bacteriophage lysogenization (51). The first gene in the *dev*
83 operon, *devI*, codes for a 40-residue protein that strongly inhibits sporulation when
84 overproduced (52), delays sporulation by about 6 h when produced at the normal level (29, 53),
85 and exerts weak positive autoregulation on *dev* transcript accumulation (29). In contrast, in-
86 frame deletions in three genes of the *dev* operon (*devTRS*) increase accumulation of the *dev*
87 transcript 10-fold during development (29, 52, 53), indicating that DevTRS proteins exert strong
88 negative autoregulation (Fig. 1). The negative autoregulation by DevTRS proteins is crucial in
89 order to prevent DevI overproduction from inhibiting sporulation (52, 53) (Fig. 1). The DevTRS

90 proteins are similar to Cas8a1, Cas7, and Cas5, respectively, of the CRISPR-associated complex
91 for antiviral defense (Cascade) (51-54).
92 The products of several other operons act late during the developmental process, impacting
93 the metabolism of nascent spores (*fadIJ*) and the biogenesis of their coat polysaccharide (*exoA-*
94 *I*, *exoL-P*, and *nfsA-H*), but the regulation of these operons is not fully understood (Fig. 1). The
95 putative *fadIJ* operon is normally induced twofold in sporulating cells, but not in *csgA*, *fruA*, or
96 *mrpC* mutants (55). Recently published data support that *fadIJ* are co-transcribed as an operon
97 (56). FadIJ are enzymes in a fatty acid β-oxidation pathway that can impact spore structure and
98 resistance properties (55). The *nfsA-H* operon is up-regulated in spores formed during the
99 starvation-induced developmental process and in spores induced artificially by glycerol addition
100 (57). The starvation-induced up-regulation fails in a *csgA* mutant, is diminished in a *devRS*
101 mutant, and, unusually, is greater in a *fruA* mutant, indicative of negative regulation by FruA
102 (57). The NfsA-H proteins form a complex involved in biogenesis of the coat polysaccharide to
103 generate compact and rigid stress-resistant spores (58-60). The *exoA-I* operon (58) is normally
104 induced late in development, but not in *csgA* or *devRS* mutants (61). Transcription depends on
105 binding of FruA (62) and Nla6 (63) to the *exoA-I* promoter region. Interestingly, Nla6 is part of a
106 cascade of enhancer-binding proteins (EBPs) that responds to starvation early in development
107 (32) and leads to production of MrpC and FruA (7) (Fig. 1). The Nla6 DNA-binding domain (DBD)
108 also binds to the promoter region of the predicted *MXAN_3259–MXAN_3263* operon and
109 appears to directly regulate transcription (63). Recently published data support that the five
110 genes are co-transcribed as an operon (56), which was renamed the *exoL-P* operon based on

111 functional studies (64). The ExoA-I and ExoL-P proteins are involved in the synthesis, export,
112 and modification of the spore coat polysaccharide (58, 59, 64).
113 Here, we report systematic investigation of the late-acting *fadIJ*, *nfsA-H*, *exoA-I*, and *exoL-P*
114 operons with respect to the phenotypes of mutants and the regulation of gene expression. We
115 found that the *nfs* and *exo* mutants exhibit defects in sporulation earlier than established
116 previously, whereas a *fad* mutant initially made more sonication-resistant spores than a "wild-
117 type" (WT) strain, but later made a similar number of mature spores. Cooperative binding of
118 MrpC and C-signal-activated FruA appears to explain up-regulation of *fadIJ* late in development,
119 but not the regulation of *nfsA-H*, *exoA-I*, and *exoL-P.* FruA negatively regulates all four operons
120 early in development and MrpC affects each operon differently. Nla6 up-regulates all four
121 operons and we discovered that its DBD binds cooperatively with FruA to the *nfsA-H*, *exoL-P*,
122 and *exoA-I* promoter regions, and also binds cooperatively with MrpC to the *nfsA-H* promoter
123 region. We also found that all four operons are subject to down-regulation by a CRISPR-Cas
124 system, especially when the DevI component is overexpressed, as in a *devS* mutant. We
125 conclude that three transcription factors and a CRISPR-Cas component regulate the late-acting
126 operons and we propose that complex, differential regulation of genes involved in spore
127 metabolism and coat biogenesis produces spores suited to withstand environmental insults.
128

129 **Results**

130 **nfs *and* exo *mutants exhibit defects early in the sporulation process***

131 In previous work, we established methods to systematically analyze *M. xanthus* development
132 under submerged culture conditions (29). Our method of submerged culture involves growing

133 cells in nutrient medium followed by sedimentation, resuspension in starvation buffer, and
134 incubation in a plastic container. Cells attach to the container bottom and develop under a
135 layer of buffer.

136 To determine the effects of mutations in the late-acting operons under our conditions of
137 submerged culture, we compared the development of mutants with that of WT laboratory
138 strain DK1622 (65) from which the mutant strains were derived. Specifically, we examined the
139 effects of an insertion in *fadI* (55), a deletion of the entire *nfsA-H* operon (57), an insertion in
140 *exoC* (58, 61), and an insertion in *exoL* (63, 64). As expected (29), the WT strain formed mounds
141 by 18 h poststarvation (PS) and the mounds began to darken by 30 h (Fig. 2). Darkening
142 typically correlates with spore formation. The *fadI* mutant was indistinguishable from the WT
143 strain. The *nfsA-H* mutant was delayed by about 3 h in mound formation and appeared to be
144 delayed and reduced in mound darkening. The *exoC* and *exoL* mutants formed normal-looking
145 mounds by 18 h, but subsequent mound darkening was reduced compared to the WT strain.

146 To quantify changes at the cellular level, we harvested samples from submerged culture and
147 either treated the samples with glutaraldehyde to fix cells or left the samples untreated (29).
148 Using the untreated samples, we quantified "sonication-resistant spores" microscopically and
149 "mature spores" that were heat- and sonication-resistant and capable of germination and
150 colony formation on nutrient agar. We used the fixed samples to quantify "sonication-sensitive
151 cells" microscopically (i.e., the total number of cells observed in the fixed sample minus the
152 number of sonication-resistant spores observed in the corresponding untreated sample). The
153 vast majority of sonication-sensitive cells were rod-shaped, but we also observed a small

154 percentage of “transitioning cells” (TCs) intermediate in morphology between rods and spores
155 (46) in some of the fixed samples.

156 As expected (29), we first observed sonication-resistant spores at 27 h PS in samples of the
157 WT strain, and the spores rose to ~2% at 48 h (Fig. 3). The *fadI* mutant formed more spores
158 than the WT strain. Consistent with the observed mound darkening defects (Fig. 2), the *nfsA-H*
159 mutant formed less spores than the WT strain, and the *exoC* and *exoL* mutants did not form
160 sonication-resistant spores (at a detection limit of 0.05%) (Fig. 3 and Table S1). Neither did the
161 *exoC* and *exoL* mutants form mature spores at 72 h (at a detection limit of 0.00001%), while the
162 *nfsA-H* mutant made ~15% as many mature spores as the WT strain, and the *fadI* mutant made
163 a similar number of mature spores as the WT strain (Table S1).

164 The WT strain exhibited a decline of sonication-sensitive cells during development similar to
165 that reported previously (29), with only ~30% of the cells remaining at 18 h PS and only ~6%
166 remaining at 48 h (Fig. S1A), presumably reflecting lysis of the majority of cells during
167 submerged culture development (3). The mutants showed similar decreases in cell number as
168 the WT strain (Fig. S1A). As noted above, we observed a small percentage of TCs in some of the
169 fixed samples. For the WT strain, ~3% of the cells were TCs at 24 h (Fig. S1B), when ~20% of the
170 cells remained (Fig. S1A). Thus, TCs comprised 15% of the total population at 24 h, before
171 sonication-resistant spores were observed (Fig. 3), in agreement with *in situ* observations using
172 confocal microscopy (46). The *fadI* mutant showed about half as many TCs as the WT strain at
173 most time points (Fig. S1B), perhaps due to the *fadI* mutant forming more sonication-resistant
174 spores (Fig. 3). The *exo* and *nfs* mutants exhibited less TCs at 24 h (~0.4-0.7%), but in each case

175 the percentage rose to at least 1% later (Fig. S1B), suggesting that these mutants begin to
176 change shape, but are impaired early in the process of making spores.
177 We conclude that the *exoC* and *exoL* mutants showed stronger defects in sporulation than
178 the *nfsA-H* mutant, whereas the *fadI* mutant initially made more sonication-resistant spores
179 than the WT strain, but later made a similar number of mature spores. All four mutants
180 exhibited less TCs than the WT strain early in the sporulation process.
181
182 ***Transcript levels from the late-acting operons are very low in the absence of C-signaling***
183 To determine the effects of loss of C-signaling on expression of the late-acting operons, we
184 used methods established previously (29) to measure transcript levels in the WT strain and a
185 *csgA* insertion mutant at 18-30 h PS, the period leading up to and including the time that many
186 cells commit to spore formation and sonication-resistant spores begin to be observed (38) (Fig.
187 3). As expected for the WT strain (39), transcript levels rose during development (Fig. 4). As
188 noted previously (53), the *exoA* transcript level varied greatly between biological replicates (Fig.
189 4A), which we do not understand. The *exoL* transcript level likewise varied greatly (Fig. 4B).
190 The *nfsA* (Fig. 4C) and *fadI* (Fig. 4D) transcript levels varied less and on average increased only
191 ~fourfold, much less than the *exoA* (~24-fold) and *exoL* (~70-fold) transcript levels.
192 In the *csgA* mutant, the transcript levels did not increase during development (Fig. 4,
193 asterisks indicate $p < 0.05$ in Student's two-tailed *t*-tests comparing the mutant to the WT strain
194 at each time point). Asterisks are absent above the *exoA* and *exoL* transcript levels of the *csgA*
195 mutant because the statistical test yielded $p > 0.05$ due to the large variation between
196 biological replicates of the WT strain. Nevertheless, the *exoA* and *exoL* transcript levels of the

197 *csgA* mutant were low for all replicates at each time point. The low transcript levels could be
198 due to decreased synthesis and/or increased degradation in the *csgA* mutant compared with
199 the WT strain. To measure the transcript degradation rates, we added rifampicin to inhibit
200 transcription at 30 h PS and determined the transcript levels at intervals thereafter. The
201 transcript degradation rates did not differ significantly between the *csgA* mutant and the WT
202 strain (Fig. 5), suggesting that decreased synthesis primarily accounts for the low transcript
203 levels in the absence of C-signaling. In agreement, reporter activity from fusions to *exoC* (61),
204 *nfsA* (57), and *fadI* (55) was very low in *csgA* mutants relative to WT strains during
205 development.

206 Considerable evidence supports a model in which C-signaling activates FruA
207 posttranslationally in order to increase transcription of genes during *M. xanthus* development
208 (28, 29). We showed previously that the FruA level is about twofold lower in the *csgA* mutant
209 than in the WT strain at 18-30 h PS (29). Boosting the FruA level in the *csgA* mutant to the WT
210 level using a vanillate-inducible promoter (P_{van}) fused to *fruA* did not increase the transcript
211 levels of five genes or operons (*dev*, *fmgA*, *fmgBC*, *fmgD*, and *fmgE*) known to be under
212 combinatorial control of FruA and MrpC. Neither did boosting the level of FruA D59E (with a
213 phosphomimetic substitution in its receiver domain) using a P_{van}-*fruA D59E* fusion.

214 We tested whether boosting the level of FruA or its D59E variant in the *csgA* mutant
215 increases the transcript levels of the late-acting operons. The transcript levels remained low in
216 all cases (Fig. S2), suggesting that neither a low level of FruA nor a lack of D59 phosphorylation
217 causes the transcript levels to remain low in the *csgA* mutant. Rather, these results are

218 consistent with evidence that C-signaling regulates FruA activity by a mechanism other than
219 phosphorylation of its receiver domain (29, 31).
220
221 ***Transcript levels from the late-acting operons are unexpectedly high in a* fruA *mutant***
222 If C-signaling activates FruA and the activated FruA increases transcription of the late-acting
223 operons, then transcript levels are expected to be low in a *fruA* insertion mutant, as observed
224 for the *dev* operon (29). Instead, the *exoA* and *exoL* transcript levels were greater in the *fruA*
225 mutant than in the WT strain at 18 to 24 h PS (Fig. 4A and 4B), and the *nfsA* transcript level in
226 the *fruA* mutant exceeded that in the WT strain at 18 h (Fig. 4C), suggesting that FruA is a
227 negative regulator of some late-acting operons early in development. In contrast, the *fadI*
228 transcript level in the *fruA* mutant was similar to that in the WT strain at 18 h and less than that
229 in the WT strain at later times (Fig. 4D), consistent with a model in which C-signaling activates
230 FruA and the activated FruA increases *fadI* transcription. Activated FruA may also increase *nfsA*
231 transcription at 27 and 30 h, since the *nfsA* transcript level in the *fruA* mutant was less than that
232 in the WT strain at those times (Fig. 4C).
233 Interestingly, the average transcript levels from the late-acting operons were greater in the
234 *fruA* mutant than in the *csgA* mutant, except for the very low *fadI* transcript level in both
235 mutants at 27 and 30 h PS (Fig. 4). As noted above, FruA is present, but its level is about
236 twofold lower in the *csgA* mutant than in the WT strain at 18-30 h (29). In the *csgA* mutant,
237 FruA is expected to remain unactivated due to the absence of C-signaling (28, 29). Therefore, it
238 is possible that unactivated FruA negatively regulates the late-acting operons in the *csgA*
239 mutant. Negative regulation by unactivated FruA may also account for the lower levels of *exoA*,

240 *exoL*, and *nfsA* transcripts we observed early in development of the WT strain as compared with
241 the *fruA* mutant (Fig. 4) (see Discussion).
242
243 ***The* exoA*, exoL, and* nfsA *transcript levels of* mrpC *and* fruA *mutants differ***
244 MrpC appears to directly stimulate transcription from the *fruA* promoter (33). In agreement,
245 FruA was not detected in an *mrpC* in-frame deletion mutant at 18-30 h PS (29). Hence, the
246 *mrpC* mutant lacks both MrpC and a detectable level of FruA. To compare the *mrpC* mutant
247 with the *fruA* mutant (lacking FruA but with MrpC present at its normal level) (29), we
248 measured the transcript levels from the late-acting operons in the mutants and the WT strain in
249 parallel. Strikingly, the *exoA*, *exoL*, and *nfsA* transcript levels in the *mrpC* and *fruA* mutants
250 differed, and in each case the pattern of effects was unique. The average *exoA* transcript level
251 was greater in the *mrpC* mutant than in the *fruA* mutant or in the WT strain at all times (Fig. 6A,
252 asterisks above brackets indicate $p < 0.05$ in Student's two-tailed *t*-tests comparing the mutants
253 at the same time point and asterisks above error bars compare a mutant to the WT strain at the
254 same time point). The comparison of mutants suggests that MrpC negatively regulates the
255 *exoA* transcript level independently of FruA, since the loss of both transcription factors in the
256 *mrpC* mutant increased the *exoA* transcript level more than loss of only FruA in the *fruA*
257 mutant. The *exoL* transcript level in the *mrpC* mutant exceeded that in the WT strain at 18 and
258 24 h, and on average exceeded that in the *fruA* mutant at 18 h, but on average was less than in
259 the *fruA* mutant at 24 h, and at 30 h the difference met a test of statistical significance (Fig. 6B).
260 In this case, comparison of the mutants suggests that, independently of FruA, MrpC negatively
261 regulates the *exoL* transcript level early in development and positively regulates it later. The

262 average *nfsA* transcript level was lower in the *mrpC* mutant than in the *fruA* mutant or in the
263 WT strain at all times (Fig. 6C), suggesting that MrpC positively regulates the *nfsA* transcript
264 level independently of FruA (i.e., opposite the regulation of *exoA*). The *fadI* transcript level was
265 lower in both mutants than in the WT strain at all times (Fig. 6D), consistent with positive
266 combinatorial control by MrpC and FruA, as observed for *dev* (42), *fmg* (31, 43-45), and likely
267 many other developmentally-regulated genes or operons (41).
268 To determine whether the lack of both MrpC and a detectable level of FruA in the *mrpC*
269 mutant affects the transcript degradation rates, we added rifampicin to inhibit transcription at
270 18 h PS and determined the transcript levels at intervals thereafter. We chose 18 h for this
271 analysis since the *exoA* (Fig. 6A) and *exoL* (Fig. 6B) transcript levels were elevated in the *mrpC*
272 mutant relative to the WT strain at that time. The transcript degradation rates did not differ
273 significantly between the *mrpC* mutant and the WT strain (Fig. S3), suggesting that increased
274 synthesis (rather than decreased degradation) primarily accounts for the elevated *exoA* and
275 *exoL* transcript levels in the *mrpC* mutant.
276
277 ***FruA can positively regulate* exoA*, exoL, and* nfsA *in the absence of MrpC***
278 To examine the effects of FruA in the absence of MrpC, we used the P_{van}-*fruA* fusion mentioned
279 previously (29) (Fig. S2) to produce FruA in the *mrpC* mutant. The inducer (vanillate) was added
280 during growth and at 0 h PS. At 6 h, the FruA level in the *mrpC* P_{van}-*fruA* mutant was about
281 threefold greater than in the WT strain, but their FruA level was similar at 12 and 18 h (Fig.
282 S4A). Interestingly, the *mrpC* P_{van}-*fruA* mutant formed immature mounds by 12 h (Fig. S5),
283 although subsequent mound darkening was reduced compared to the WT strain (Fig. S6) and

284 spores were not detected (Table S1). Nevertheless, mound formation suggests that C-signaling
285 is activating FruA to some extent, since a complete block, as in *mrpC*, *fruA*, and *csgA* mutants,
286 results in no mound formation (29) (Fig. S5).

287 To determine the effects of FruA on regulation of the late-acting operons in the absence of
288 MrpC, we measured the transcript levels in the *mrpC* P_{van}-*fruA* mutant in parallel with those in
289 the *mrpC* and *fruA* mutants and the WT strain at 6-18 h PS. We chose to collect samples during
290 that period of development since FruA was present (Fig. S4A) and appeared to be active (Fig.
291 S5) in the *mrpC* P_{van}-*fruA* mutant and the WT strain, as described above. The *exoA* (Fig. 7A) and
292 *exoL* (Fig. 7B) transcript levels in the *mrpC* P_{van}-*fruA* mutant exceeded those in the WT strain at
293 all times, and on average exceeded those in the *mrpC* and *fruA* mutants, except the *exoL*
294 transcript level in the *mrpC* mutant was similar to that in the *mrpC* P_{van}-*fruA* mutant at 18 h.
295 We conclude that FruA can positively regulate the *exoA* and *exoL* transcript levels in the
296 absence of MrpC. This regulation may involve C-signal-activated FruA since the *mrpC* P_{van}-*fruA*
297 mutant formed immature mounds (Fig. S5 and S6), whereas *mrpC*, *fruA*, and *csgA* mutants fail
298 to form mounds (29) (Fig. S5). The *nfsA* transcript level in the *mrpC* P_{van}-*fruA* strain exceeded
299 that in the WT strain at 6 h and that in the *mrpC* mutant at 6 and 12 h (Fig. 7C), also indicative
300 of positive regulation by FruA (perhaps activated FruA) in the absence of MrpC. On the other
301 hand, the *fadI* transcript level in the *mrpC* P_{van}-*fruA* strain was less than that in the WT strain
302 (Fig. 7D), as observed for the *mrpC*, *fruA*, and *csgA* mutants (Fig. 4D, 6D, and 7D), supporting
303 that positive regulation requires both MrpC and activated FruA.

304

305 ***Nla6 positively regulates the transcript levels of the late-acting operons***

306 The Nla6 transcription factor appears to be a direct regulator of the *exoA-I* and *exoL-P* operons
307 since a protein with the *E. coli* maltose-binding protein (MBP) fused to the Nla6 DBD (MBP-Nla6
308 DBD) bound to promoter region DNA fragments (63). A comparison of the *exoA* and *exoL*
309 transcript levels in an *nla6* insertion mutant and a WT strain suggested that Nla6 positively
310 regulates both during the first 8 h PS, and negatively regulates both at 24 h (63). To facilitate
311 planned strain construction, we constructed a new *nla6* insertion mutant and compared it with
312 the one characterized previously (63, 66). The new mutant is tetracycline-resistant (Tc^r) and
313 the one described previously is kanamycin-resistant (Km^r). Both mutants formed immature
314 mounds by 12 h, but failed to progress to more mature mounds with distinct, round edges by
315 18 h (Fig. S5). Later during development, the Km^r *nla6* mutant mounds matured somewhat at
316 24-30 h, but failed to darken by 36-48 h (Fig. S6). The Tc^r *nla6* mutant mounds did not mature
317 until 36 h and also failed to darken by 48 h. Spores were not detected for either mutant (Table
318 S1).
319 The two *nla6* mutants were indistinguishable in terms of the molecular markers we tested.
320 Since our results showed that FruA and MrpC impact transcript levels of the late-acting operons
321 at 18 h PS (Fig. 4 and 6) and in some cases earlier during development (Fig. 7), we measured the
322 levels of FruA, MrpC, and transcripts from the late-acting operons in the *nla6* mutants and the
323 WT strain at 6-18 h. The FruA and MrpC protein levels in the *nla6* mutants were similar to
324 those in the WT strain at 6-18 h (Fig. S4). The *exoA*, *nfsA*, and *fadI* transcript levels in the WT
325 strain increased at 18 h, but those in the *nla6* mutants failed to increase (Fig. 8), suggesting that
326 Nla6 positively regulates those transcript levels. The *exoL* transcript level in the WT strain did
327 not increase at 18 h, but on average that in the *nla6* mutants was less (Fig. 8B), suggesting that

328 Nla6 also positively regulates the *exoL* transcript level. Because the *exoA*, *exoL*, and *nfsA*
329 transcript levels of the *mrpC* and/or *fruA* mutants exceeded those of the WT strain early in
330 development (Fig. 4, 6, and 7), we tried to construct *mrpC nla6* and *fruA nla6* double mutants,
331 but our efforts were unsuccessful, so we were unable to determine whether positive regulation
332 by Nla6 could account for the elevated transcript levels in the *mrpC* and *fruA* mutants relative
333 to the WT strain.
334
335 ***Binding of MBP-Nla6 DBD, MrpC, and FruA differs at the promoter region of each of the late-***
336 ***acting operons***
337 As a possible indication of direct regulation by Nla6, MrpC, and FruA, we tested for binding to a
338 DNA fragment upstream of the predicted start codon of the first gene in each of the late-acting
339 operons. Figure S7 shows features of each promoter region fragment based on previous work.
340 FruA and MrpC were shown to bind cooperatively to the *dev* promoter region fragment (42)
341 (Fig. S7A), which was used here as a control. The FruA DBD was shown to bind to at least two
342 sites in the *exoA-I* promoter region fragment (62) and MBP-Nla6 DBD was also shown to bind,
343 presumably *via* interaction with DNA sequences similar to a half-site consensus sequence (63)
344 (Fig. S7B). MBP-Nla6 DBD was also shown to bind to the *exoL-P* promoter region fragment (63)
345 and three matches to the half-site consensus sequence were identified (Fig. S7C). ChIP-seq
346 analysis suggested that MrpC binds to a site upstream of *nfsA-H* at 18 h PS (41) (Fig. S7D). Here,
347 we used electrophoretic mobility shift assays (EMSAs) to test for binding of purified MBP-Nla6
348 DBD, MrpC, and FruA separately, and in combination because MrpC and FruA were shown

349 previously to bind cooperatively to the promoter regions of *dev* (42), *fmg* (31, 43-45), and other
350 developmentally-regulated genes or operons (41).
351 As expected (42), MrpC and FruA bound individually to the *dev* promoter region fragment
352 (Fig. 9A, lanes 4, 5, 7, 8), and the combination of MrpC and FruA exhibited greater than additive
353 binding (lanes 11, 14), indicative of cooperative binding. MrpC and FruA DBD also appeared to
354 bind cooperatively (Fig. S8A, lane 4), indicating the N-terminal domain of FruA was not
355 required. Binding of MBP-Nla6 DBD was not detected at 4 μM (Fig. 9A, lane 2), consistent with
356 previous reports (32, 63), but binding was detected at 16 μM and increased at greater
357 concentrations (Fig. S8A, lanes 8-10).
358 The *fadIJ* promoter region fragment yielded results that were in some ways similar to those
359 for the *dev* fragment. MrpC and FruA bound individually to the *fadIJ* fragment (Fig. 9B, lanes 3,
360 4), and the combination of MrpC and FruA appeared to bind cooperatively (lane 7), but with
361 much less cooperative binding than to the *dev* fragment. The order of MrpC and FruA addition
362 did not affect cooperative binding to either fragment (Fig. 9A, lanes 11, 14 and Fig. S8B, lanes 5,
363 6). However, MrpC and FruA DBD did not bind cooperatively to the *fadIJ* fragment (Fig. S8B,
364 lane 10), indicating a requirement for the FruA N-terminal domain, in contrast to the *dev*
365 fragment. On the other hand, for both fragments, MBP-Nla6 DBD binding was not detected at
366 4 μM and at that concentration did not affect binding of MrpC or FruA (Fig. 9A, lanes 2, 9, 10,
367 12, 13 and Fig. 9B, lanes 2, 5, 6). Also like the *dev* fragment, MBP-Nla6 DBD binding to the *fadIJ*
368 fragment was detected at 16 μM and increased at higher concentrations (Fig. S8B, lanes 14-16).
369 The apparent cooperative binding of MrpC and FruA to the *fadIJ* fragment, together with our
370 measurements of the *fadI* transcript level, support a similar mechanism of developmental

371 regulation of the *fadIJ* operon as proposed for the *dev* operon (29, 42), the *fmg* genes (31, 43-
372 45), and likely many other genes (41), in which C-signaling activates FruA to bind DNA
373 cooperatively with MrpC and increase transcription.

374 MBP-Nla6 DBD at 2 μM bound to the *exoA-I* promoter region fragment (Fig. 9C, lane 2), as
375 expected (63). FruA also bound (Fig. 9C, lanes 7, 8), as expected based on FruA DBD binding
376 observed previously (62). Strikingly, MBP-Nla6 DBD and FruA appeared to bind cooperatively
377 and the order of addition made no difference (Fig. 9C, lanes 10, 13 and Fig. S8C, lanes 4-6).
378 FruA DBD exhibited very little cooperative binding with MBP-Nla6 DBD (Fig. S8C, lane 10),
379 suggesting the N-terminal domain of FruA plays an important role. Although MrpC appeared to
380 negatively regulate the *exoA* transcript level independently of FruA (Fig. 6A), binding of MrpC
381 was not detected at 4 μM (Fig. 9C, lane 5) or at concentrations ranging up to 20 μM (Fig. S8C,
382 lanes 12-16), and MrpC did not affect MBP-Nla6 DBD or FruA binding (Fig. 9C, lanes 9, 11, 12,
383 14). Taken together, our results suggest that MrpC regulates *exoA* indirectly both
384 independently of FruA (Fig. 6A) and because MrpC is required for synthesis of FruA (29, 62),
385 which appears to bind cooperatively with Nla6 to the promoter region and increase *exoA-I*
386 transcription.

387 We discovered that FruA binds to the *exoL-P* promoter region fragment (Fig. 9D, lane 4).
388 Binding of MBP-Nla6 DBD was not detected at 4 μM in the experiment shown in Figure 9D (lane
389 2), but was detected at 4 μM in two other experiments (Fig. S8D, lanes 2, 8). Interestingly,
390 MBP-Nla6 DBD and FruA appeared to bind cooperatively and the order of addition made no
391 difference (Fig. 9D, lane 6 and Fig. S8D, lanes 4-6), similar to our results for the *exoA-I* fragment.
392 Both fragments also yielded similar results in other experiments; FruA DBD exhibited very little

393 cooperative binding with MBP-Nla6 DBD to the *exoL-P* fragment (Fig. S8D, lane 10) and MrpC
394 did not affect MBP-Nla6 DBD or FruA binding (Fig. 9D, lanes 5, 7). However, the two fragments
395 differed in terms of MrpC binding, which was not detected for the *exoA-I* fragment at MrpC
396 concentrations ranging up to 20 μM (Fig. S8C, lanes 12-16). In contrast, for the *exoL-P*
397 fragment, although binding of MrpC was not detected at 4 μM in the experiment shown in
398 Figure 9D (lane 3), binding was detected at 4 μM and increased at higher concentrations in
399 another experiment (Fig. S8D, lanes 12-16). Therefore, MrpC (as well as FruA and Nla6, which
400 bind cooperatively) appears to directly regulate *exoL-P*, differentiating its regulation from that
401 of *exoA-I* (see Discussion).
402 We found that MBP-Nla6 DBD, MrpC, and FruA could each bind individually to the *nfsA-H*
403 promoter region fragment (Fig. 9E, lanes 2-7). In combination with MBP-Nla6 DBD at 4 μM,
404 individual binding of MrpC was not detected and the intensity of the shifted complex increased
405 at the lagging edge (Fig. 9E, lane 9), suggestive of cooperative binding. In agreement, MBP-Nla6
406 DBD at 2 μM appeared to bind cooperatively with MrpC, and the order of addition made little
407 or no difference (Fig. S8E, lanes 4-6). We note that the large sizes of MBP-Nla6 DBD and the
408 DNA fragment likely explain the small difference in migration of the putative MBP-Nla6
409 DBD/MrpC/DNA complex compared to the MBP-Nla6 DBD/DNA complex (Fig. S8E, lanes 2, 4-6).
410 Like MrpC, FruA appeared to bind cooperatively with MBP-Nla6 DBD (Fig. 9E, lane 10 and Fig.
411 S8E, lanes 10-12). In the mixtures with MBP-Nla6 DBD, individual binding of FruA was detected,
412 suggestive of less cooperativity than in the case of MrpC. FruA DBD did not appear to bind
413 cooperatively MBP-Nla6 DBD (Fig. S8E, lane 16), and FruA did not appear to bind cooperatively
414 with MrpC (Fig. S8E, lanes 20-22). We conclude that MBP-Nla6 DBD, MrpC, and FruA appear to

415 directly regulate *nfsA-H* and we note that the apparent cooperative binding of MBP-Nla6 DBD
416 and MrpC to the *nfsA-H* fragment distinguishes it from the *exoA-I* and *exoL-P* fragments.
417 Altogether, the results of our EMSAs and transcript measurements suggest that *fadIJ*
418 regulation is similar to that of *dev* (42), *fmg* (31, 43-45), and likely many other genes or operons
419 (41), involving cooperative binding of MrpC and C-signal-activated FruA. In contrast, regulation
420 of the other late-acting operons appears to involve cooperative binding of Nla6 and FruA, and
421 MrpC acting indirectly (*exoA-I*), directly but not binding cooperatively with Nla6 or FruA (*exoL-*
422 *P*), or binding cooperatively with Nla6 (*nfsA-H*).
423
424 ***DevI negatively regulates the transcript levels of the late-acting operons***
425 Reporter activity from fusions to *exoC* (61) and *nfsA* (57) was reduced in a *devRS* insertion
426 mutant compared with a WT strain during development. The *exoA* transcript level was also
427 reduced in a *devS* in-frame deletion mutant compared with a WT strain during development
428 (53). To further investigate the effects of mutations in the *dev* operon, which comprises a
429 CRISPR-Cas system (51), on regulation of the late-acting operons, we measured transcript levels
430 in *devI* and *devS* in-frame deletion mutants. Sporulation occurs about 6 h earlier than normal in
431 the *devI* mutant (29, 53), suggesting that DevI delays sporulation of the WT strain. Sporulation
432 is severely impaired in the *devS* mutant (29, 51) due to loss of negative autoregulation of *dev*
433 transcription and resulting overproduction of DevI, which strongly inhibits sporulation (52).
434 We found that the *exoA*, *exoL*, *nfsA*, and *fadI* transcript levels remain low in the *devS*
435 mutant at 18-30 h PS (Fig. 10). We infer that DevI overproduction in the *devS* mutant inhibits
436 accumulation of transcripts from the late-acting operons. Although Student's two-tailed *t*-tests

437 rarely yielded $p < 0.05$ comparing transcript levels in the *devS* mutant with the WT strain at the
438 corresponding time PS, this was due to the large variation between biological replicates of the
439 WT strain. We emphasize that transcript levels were low in all biological replicates of the *devS*
440 mutant at all times PS.

441 The average transcript levels were greater in the *devI* mutant than the WT strain, except the
442 *nfsA* transcript level was similar in both at 30 h PS (Fig. 10). These results are consistent with
443 the notion that DevI inhibits accumulation of transcripts from the late-acting operons. Here
444 again, Student's two-tailed *t*-tests rarely yielded $p < 0.05$, but in this case there was large
445 variation between biological replicates of both the *devI* mutant and the WT strain. Even so,
446 taken together, the measurements of transcript levels in the *devI* and *devS* mutants support
447 that DevI is a negative regulator of the late-acting operons.

448

449 **Discussion**

450 We investigated the function and regulation of genes whose products act near the end of the
451 *M. xanthus* developmental process to change metabolism of the spore and protect its contents
452 by depositing a polysaccharide coat on its surface. We found that the *exoA-I*, *exoL-P*, and *nfsA-*
453 *H* operons involved in spore coat biogenesis impact the formation of resistant spores earlier
454 than shown previously, but do not prevent the initial cellular shape change associated with
455 sporulation. We discovered that the regulation of the late-acting operons is unusually complex.
456 It involves three transcription factors that bind to the promoter regions in different
457 combinations, allowing each promoter to be regulated uniquely. Combinatorial regulation of
458 this complexity is common in higher eukaryotes (67-69), but not in bacteria. Our results also

459 show that the late-acting operons are controlled by a CRISPR-Cas system. These systems
460 typically defend bacteria against viral infection, but are often repurposed for a variety of
461 functions, including regulation of endogenous gene expression (70, 71). Collectively, our results
462 suggest that *M. xanthus* evolved complex eukaryotic-like combinatorial control of transcription
463 and a link to a CRISPR-Cas system to thwart viral intrusion while making spores suited to
464 withstand starvation and environmental insults.
465
466 ***New insights into the functions of the late-acting operons***
467 Our results show that mutations in *exoC*, *nfsA-H*, and *exoL* reduce the formation of sonication-
468 resistant spores beginning at 27 h PS (Fig. 3), but do not prevent the initial cellular shape
469 change associated with starvation-induced sporulation (Fig. S1B). Previously, these mutants
470 were examined for sporulation at 120 h (58, 63, 64). Our findings indicate a much earlier role of
471 the ExoA-I, NfsA-H, and ExoL-P proteins during development than established previously. The
472 *nfsA-H* mutant made about twofold less sonication-resistant spores than the WT strain at 27-48
473 h, whereas the *exoC* and *exoL* mutants made less than the detection limit (Fig. 3). The milder
474 sporulation defect of the *nfsA-H* mutant compared with the *exoC* and *exoL* mutants (Fig. 3 and
475 Table S1) is consistent with previous reports (58, 63, 64). The *exoC* mutant fails to export spore
476 coat polysaccharide, whereas the *nfsA-H* mutant appears to export it, but fails to assemble it
477 properly, producing an amorphous, unstructured coat that nevertheless appears to provide
478 some heat- and sonication-resistance (58). The *fadI* mutant made about twofold more
479 sonication-resistant spores than the WT strain (Fig. 3). The *fadI* insertion mutant presumably

480 has a reduced rate of fatty acid β-oxidation (55), so perhaps altered metabolism enhanced
481 formation of sonication-resistant spores (Fig. 3), albeit not mature spores at 72 h (Table S1).
482 Building on the recent observation of TCs in nascent fruiting bodies (46), we devised a
483 method that allowed us to visualize and enumerate TCs in samples of the starved mutants (Fig.
484 S1B). These TCs likely resemble cells of *exo* and *nfs* mutants that fail to complete
485 morphogenesis upon chemical induction of sporulation in liquid culture (58, 59, 64). The lower
486 percentage of TCs we observed for *exoC*, *nfsA-H*, and *exoL* mutants as compared with the WT
487 strain at 24 and 27 h (Fig. S1B) may reflect reduced ability to initiate and/or maintain the
488 cellular shape change associated with sporulation.
489
490 ***Combinatorial regulation by three signal-responsive transcription factors links expression of***
491 ***late-acting operon to environmental conditions***
492 Eukaryotic-like signaling and gene regulation have been known in *M. xanthus* for decades (72,
493 73). More recently, combinatorial control, a common theme in eukaryotic GRNs (67-69),
494 emerged from studies of *M. xanthus* gene regulation (7, 35). Combinatorial control allows
495 signal integration by utilizing two or more signal-responsive transcription factors to directly
496 regulate the same gene. Our transcript measurements demonstrate unique regulation of each
497 late-acting operon and our DNA-binding assays implicate combinatorial control of each
498 promoter region by two or three transcription factors (Fig. 11). The late-acting operons are
499 shown twice to indicate differential regulation early (~6-18 h PS) and late (~21-30 h) in
500 development (gray boxes at right). The early period approximates when mound formation
501 occurs in the WT strain (Fig. 2, S5, S6, and the cartoon at left in Fig. 11). The late period

502 includes times leading up to and including the beginning of sporulation (Fig. 3 and 11). Our
503 transcript measurements focused on the early (Fig. 7 and 8) or late (Fig. 4, 6, 10, and S2) period
504 and both included 18 h. The results show that transcript levels began to increase markedly by
505 18 h (*exoA*, *nfsA*, and *fadIJ*) or 24 h (*exoL*) and continued to increase until 30 h. For simplicity,
506 our model ignores this difference in timing of transcript increase and we focus primarily on
507 explaining negative regulation during the early period and positive regulation during the late
508 period. In the model, green arrows and red lines with a barred end indicate positive and
509 negative regulation, respectively, based on our transcript measurements. Solid versus dashed
510 arrows/lines represent our interpretation of our EMSA results as indicative of direct versus
511 indirect regulation. We interpret binding of transcription factors at relatively low
512 concentrations (≤ 4 μM) to a promoter region fragment as indicative of direct regulation, and
513 either no detectable binding or binding at relatively high concentrations (≥ 16 μM) as indicative
514 of indirect regulation. Cartoons below the operons in the model also take into account our
515 DNA sequence analysis of potential binding sites for the transcription factors (Fig. S9), in an
516 effort to illustrate how independent, cooperative, and competitive binding could explain the
517 complex regulation observed. Importantly, much more work will be required to test our model.
518 For example, binding sites will need to be identified and mutated, and the effects on
519 transcription measured.

520 To explain negative regulation of the late-acting operons early in development, our model
521 proposes that unactivated FruA directly opposes stimulation of transcription by Nla6-P at the
522 *exoA-I*, *exoL-P*, and *nfsA-H* promoter regions (Fig. 11). This model could explain a large increase
523 in the *exoA-I* and *exoL-P* transcript levels between 0 and 1 h PS followed by a comparable

524 decrease by 12 h in a WT strain (63). FruA is present at 6 h and its level increases threefold by
525 12 h (Fig. S4A). FruA* appears to be present by 18 h (29), but the kinetics of FruA activation are
526 unknown. Presumably, mound formation brings cells into proximity, enabling C-signal-
527 dependent activation of FruA (19, 46), so FruA* increases and unactivated FruA decreases
528 during mound formation, which occurs primarily between 12 and 18 h under our conditions
529 (Fig. S5). Therefore, we expect unactivated FruA to be abundant by 6 h (possibly earlier),
530 perhaps opposing Nla6-P stimulation after the initial increase of *exoA-I* and *exoL-P* transcript
531 levels (63).

532 Our model proposing negative regulation by unactivated FruA early in development (Fig. 11)
533 is consistent with two prior reports of negative regulation by FruA. Expression of a reporter
534 fused to the *nfsA-H* promoter region was elevated in a *fruA* mutant compared with a WT strain
535 at 12-18 h PS (57). While our work was in progress, transcriptomic analysis identified > 1500
536 genes with an elevated transcript level in the *fruA* mutant compared to the WT strain at 12 h
537 (6). Based on the data of McLoon *et al.* (6), the transcript levels of all genes in the late-acting
538 operons were elevated in the *fruA* mutant relative to the WT strain at 12 h (Table S2). In our
539 study, the *exoA-I*, *exoL-P*, and *nfsA-H* transcript levels were elevated in the *fruA* mutant relative
540 to the WT strain at 18 h (Fig. 4, 6, and 7), but not at 12 h (Fig. 7), suggesting a temporal
541 difference in development between the studies. The *fadI* transcript level was lower in the *fruA*
542 mutant than in the WT strain at all times tested in our experiments (Fig. 4D, 6D, and 7D), but its
543 level in the *fruA* mutant exceeded that in the *csgA* mutant by a small, reproducible amount at
544 18 h (Fig. 4D, $p = 0.002$ in a Student's two-tailed *t*-test), supporting weak negative regulation by
545 unactivated FruA (Fig. 11). Our model proposes that unactivated FruA directly opposes

546 stimulation of *fadIJ* transcription by cooperative binding of MrpC and FruA* early in
547 development (Fig. 11 cartoon), rather than opposing stimulation by Nla6-P, for two reasons.
548 First, a high concentration of MBP-Nla6 DBD was required to detect binding to the *fadIJ*
549 promoter region fragment (Fig. S8B), suggesting indirect regulation by Nla6-P (Fig. 11). Second,
550 our analysis revealed potential binding sites for MrpC and FruA or FruA*, but not for Nla6,
551 upstream of the *fadIJ* promoter (Fig. S9A).

552 Our model also proposes that MrpC affects transcription of the *exoA-I*, *exoL-P*, and *nfsA-H*
553 operons early in development (Fig. 11). The *exoA* transcript level was on average at least
554 twofold greater in the *mrpC* mutant than the *fruA* mutant at 18 h PS (Fig. 6A and 7A),
555 suggesting negative regulation by MrpC independently of FruA, but we did not detect MrpC
556 binding to the *exoA-I* promoter region fragment (Fig. S8C) or potential binding sites (Fig. S9D).
557 Therefore, we propose that MrpC indirectly decreases transcription of the *exoA-I* operon early
558 in development of the WT strain (Fig. 11). In contrast, our results imply that MrpC directly
559 decreases *exoL-P* transcription and directly increases that of *nfsA-H* early in development (Fig.
560 6, 7, 9, S8, and 11).

561 The cartoons below the *exoA-I*, *exoL-P*, and *nfsA-H* operons in Figure 11 propose that
562 unactivated FruA and MrpC engage in cooperative or competitive binding with Nla6-P or each
563 other primarily to inhibit transcription early in development of the WT strain. Our EMSAs (Fig.
564 9 and S8) and our analysis revealing adjacent potential binding sites (Fig. S9) support the
565 cooperative binding depicted. We infer competitive binding at overlapping potential binding
566 sites (Fig. S9). The arrangement of transcription factors in the cartoons (Fig. 11) mimics the
567 arrangement of potential binding sites (Fig. S9) proposed to play important roles (Supporting

568 Information, additional discussion). Not all the potential binding sites shown in Figure S9 are
569 depicted in the Figure 11 cartoons.
570 To explain positive regulation of the late-acting operons late in development, our model
571 proposes that C-signaling switches FruA from a negative regulator to a positive regulator, FruA*
572 (Fig. 11). The switch is most evident comparing the *nfsA* transcript levels in the *fruA* mutant
573 with those in the WT strain as development proceeds (i.e., the transcript level increases in the
574 WT strain and decreases in the *fruA* mutant) (Fig. 4C). The switch is less evident from a
575 comparison of *exoA* transcript levels due to large variation between biological replicates of the
576 WT strain late in development, but on average the transcript level increases in the WT strain
577 and decreases in the *fruA* mutant (Fig. 4A). Our findings that ectopic FruA expression in the
578 *mrpC* mutant allowed formation of immature mounds (Fig. S5) and greatly increased the *exoA*
579 transcript level (Fig. 7A) also support a switch to stimulation of transcription by FruA* (Fig. 11).
580 Similar findings suggest that FruA* increases the *exoL* transcript level (Fig. 7B and 11).
581 However, the *exoL* transcript level does not decrease in the *fruA* mutant late in development
582 (Fig. 4B). Therefore, we propose that MrpC can act as a direct positive regulator independently
583 of FruA* (Fig. 11). In contrast, our results suggest that cooperative binding of MrpC and FruA*
584 stimulates *fadIJ* transcription late in development (Fig. 11).
585 The cartoons in Figure 11 shown below the operons late in development reflect our EMSA
586 results (Fig. 9 and S8) and our analysis of potential binding sites (Fig. S9), using similar reasoning
587 as explained above, except we propose that FruA* may differ from unactivated FruA in terms of
588 affinity for potential binding sites and the effect of cooperative binding with Nla6-P or
589 dephosphorylated Nla6 (Supporting Information, additional discussion). In short, we propose

590 that MrpC and FruA* bind cooperatively near the *fadIJ* promoter to stimulate transcription late
591 in development, whereas binding of MrpC and unactivated FruA farther upstream weakly
592 inhibits transcription stimulation earlier (Fig. 11 cartoons). The cartoons below the *exoA-I*,
593 *exoL-P*, and *nfsA-H* operons propose that FruA* and MrpC bind independently and/or engage in
594 cooperative or competitive binding with Nla6-P (or dephosphorylated Nla6, which is not shown
595 for simplicity) primarily to stimulate transcription late in development of the WT strain.
596 We conclude that each late-acting operon is uniquely regulated by two or three
597 transcription factors acting combinatorially. The positions and affinities of binding sites for
598 Nla6-P or dephosphorylated Nla6, MrpC, and FruA or activated FruA* in each promoter region
599 determine the transcriptional output from independent, cooperative, and competitive binding.
600 This regulatory complexity was masked in transcriptomic studies. The four late-acting operons
601 we investigated were clustered in one (5) or two (4, 6) groups with hundreds of other genes,
602 but our transcript measurements in several mutants revealed unique regulation of each operon
603 (Fig. 4, 6, and 7), our DNA-binding assays showed different binding of transcription factors to
604 each promoter region (Fig. 9 and S8), and our analysis of potential binding sites uncovered
605 diverse, complex architectures (Fig. S9). Collectively, our results and the transcriptomic studies
606 predict that tremendous regulatory complexity will be uncovered by genome-wide
607 measurements of transcript levels in mutants, transcription factor binding studies, and
608 bioinformatic analyses.
609 Since combinatorial control allows signal integration, what are the signals to which the late-
610 acting operons respond? Starvation triggers a cascade of EBPs that includes Nla6-P and Nla28-P
611 (32), and leads to the production of MrpB-P (74), another EBP that in turn leads to production

612 of MrpC (75) (Fig. 11). However, more specific molecular signals controlling these steps are
613 unknown. In particular, it is unknown whether Nla6 responds to different signals early and late
614 in development, or how it switches from positive to negative regulation of the *exo* operons (63)
615 (Fig. 11). Nutrients and an unknown signal sensed by the Esp system stimulate proteolysis of
616 MrpC (Fig. 11) to delay or halt development (36-39). The presumed advantage of such a
617 developmental checkpoint is to ensure that cellular physiology and interactions with other cells,
618 as well as environmental conditions, warrant commitment to spore formation (38, 76, 77). C-
619 signaling appears to require the movement of cells into alignment or possibly into contact, and
620 lead to the formation of active FruA* (18-20, 28, 29, 46). Early in development, unactivated
621 FruA appears to function as a global negative regulator (6) (Fig. 11), preventing premature
622 production of some proteins that would be detrimental during mound formation (e.g., Nfs and
623 Exo proteins involved in polysaccharide export), in addition to conserving cellular resources.
624 Altogether, our knowledge about the specific signals to which the late-acting operons respond
625 is quite limited, but in general, nutrient limitation and movement of cells into proximity appear
626 to play important roles, and are likely influenced by many other factors in the environment of
627 the developing population.
628 We propose that combinatorial control of the late-acting operons and hundreds of other
629 genes by signal-responsive transcription factors allows proper temporal and spatial expression
630 of genes involved in spore metabolism, coat biogenesis, and other functions in order to
631 produce spores that are densely packed in fruiting bodies and suited to withstand
632 environmental insults. Numerous studies show that environmental conditions affect the
633 resistance and surface characteristics of endospores from *Bacillus* species (78-80). In *Bacillus*

634 *subtilis*, several transcription factors positively and negatively fine-tune the expression of
635 hundreds of genes during sporulation (81-83), ensuring that the resulting spores are endowed
636 with resistance and surface properties tailored for their environment (84-86). Understanding
637 how ecology and evolution impact the developmental GRN of *M. xanthus* and related species is
638 an ongoing and future challenge (6, 87, 88).
639
640 ***The DevI component of a CRISPR-Cas system is a negative regulator of the late-acting operons***
641 Our results confirm and extend the role of DevI as a negative regulator of late-acting operons
642 during development. We confirmed that the *exoA* transcript level is very low in the *devS* null
643 mutant (53) and we observed similar results for the *exoL*, *nfsA*, and *fadI* transcript levels (Fig.
644 10). The cumulative effect of failure to express the late-acting operons may explain the inability
645 of the *devS* mutant to undergo normal cellular shape change (53). Alternatively, one or more
646 other genes subject to negative regulation by DevI overproduction may be responsible. We
647 also found that transcript levels from the late-acting operons were slightly greater on average
648 in a *devI* mutant than in the WT strain, supporting our conclusion that DevI is a negative
649 regulator of the late-acting operons (Fig. 11); however, the mechanism of negative regulation
650 by DevI is unknown.
651 The *dev* CRISPR-Cas system appears to have evolved recently (52), perhaps in niches where
652 protection from bacteriophage infection and/or delayed sporulation were advantageous (51,
653 53). Most natural isolates of *M. xanthus* lack *devI* and their *dev* promoter region is predicted to
654 be nonfunctional (52). The *dev* operon is dispensable for development of the WT laboratory
655 strain used in this work (53). However, the *dev* CRISPR-Cas system may protect against

656 intrusion by bacteriophage Mx8 during development, since a 37-bp sequence in the CRISPR
657 matches a sequence in the Mx8 integrase gene (51). This hypothesis remains to be tested, as
658 do the potential benefits of such protection.
659 In summary, our investigation uncovered complex regulation of genes involved in spore
660 metabolism and spore coat biogenesis by three transcription factors and a CRISPR-Cas
661 component during *M. xanthus* development. Further elucidating the signals to which Nla6,
662 MrpC, and FruA respond, understanding how these transcription factors interact at promoter
663 regions, and elucidating how DevI inhibits the cellular shape change associated with sporulation
664 are important goals for the future.
665
666 **Experimental procedures**
667 ***Bacterial strains, plasmids and primers***
668 The strains, plasmids and primers used in this study are listed in Table S3.
669 *M. xanthus* strain MSS2 with P_{van}-*fruA* integrated ectopically was constructed by
670 electroporating (89) pSS10 into strain DK1622, selecting transformants on CTT agar (1%
671 Casitone, 10 mM Tris-HCl [pH 8.0], 1 mM KH_2PO_4-K_2HPO_4, 8 mM $MgSO_4$ [final pH 7.6] solidified
672 with 1.5% agar) containing 15 μg/mL tetracycline (90), and verification by colony PCR using
673 primers pMR3691 MCS G-F and pMR3691 MCS G-R.
674 *M. xanthus* strain MSS10 with a plasmid insertion mutation in *nla6* was constructed by
675 electroporating pSS11 into strain DK1622, selecting transformants on CTT agar containing
676 tetracycline (15 μg/mL), and verification by colony PCR using primers PMR3487 Rev, Nla6 Fwd4,
677 and Nla6 Fwd5. To construct pSS11, primers Nla6 Fwd and Nla6 Rev were used to generate a

678 PCR product using chromosomal DNA from *M. xanthus* strain DK1622 as a template. The
679 product was combined with DNA amplified from pMR3487 using primers PMR3487G Fwd and
680 PMR3487G Rev primers, and a Gibson assembly reaction was used to enzymatically join the
681 overlapping DNA fragments (91). The reaction mixture was transformed into *E. coli* strain
682 DH5α, transformants were selected at 37°C on Luria-Bertani (LB) (92) 1.5% agar containing 15
683 μg/mL tetracycline, and the cloned DNA sequence was verified using primers 3487 seq Fwd1,
684 3487 seq Fwd2, 3487 seq Fwd3, 3487 seq Fwd4, and 3487 seq Fwd5.
685 To provide a DNA template for amplification of the *nfsA-H* promoter region, pSS14 was
686 constructed as follows. Primers Nfs -290G and Nfs +83G were used to generate a PCR product
687 using chromosomal DNA from *M. xanthus* strain DK1622 as a template. The product was
688 combined with DNA amplified from pMR3487, the overlapping DNA fragments were joined
689 using a Gibson assembly reaction, the reaction mixture was transformed into *E. coli* strain
690 DH5α, transformants were selected, and the cloned DNA sequence was verified as described
691 above for pSS11.
692 To express MBP-Nla6 DBD for purification, primers Nla DBD For and Nla DBD Rev were used
693 to generate a PCR product using *nla6* DNA as a template. The PCR product was digest with *Sbf*I
694 and ligated to *Xmn*I-*Sbf*I-digested pMAL-c5x (NEB), resulting in pMAL-c5x/MBP-ΔCNla6 DBD,
695 which lacked a CG bp at the beginning of the Nla6 DBD-encoding segment. The missing CG bp
696 was added by performing site-directed mutagenesis using the QuikChange strategy (Stratagene)
697 with primers MBP-Nla6 add C fwd and MBP-Nla6 add C rev, resulting in pMAL-c5x/MBP-Nla6
698 DBD, and the DNA sequence was verified using primer mbp fwd colpcr.
699

700 ***Growth and development of* M. xanthus**

701 Strains of *M. xanthus* were grown at 32°C in CTTYE liquid medium (CTT medium with 0.2% yeast
702 extract) with shaking at 350 rpm. CTT agar was used for growth on solid medium and was
703 supplemented with 40 μg/mL of kanamycin sulfate or 15 μg/mL of tetracycline as required.
704 Fruiting body development under submerged culture conditions was performed using MC7 (10
705 mM morpholinepropanesulfonic acid [MOPS; pH 7.0], 1 mM $CaCl_2$) as the starvation buffer as
706 described previously (38). Briefly, cells in the mid-exponential phase of growth were collected
707 by centrifugation, the supernatant was removed, and the cells were resuspended in MC7 buffer
708 at a density of approximately 1,000 Klett units. A 96-μL sample (designated T_0) was removed
709 and 4 μL of glutaraldehyde was added from a 50% stock solution to achieve a 2% final
710 concentration. The sample was stored at 4°C for at least 24 h in order to fix the cells for later
711 quantification of total cells as described below. For each developmental sample, 1.5 mL of the
712 1,000-Klett-unit cell suspension plus 10.5 mL of MC7 buffer was added to an 8.5-cm-diameter
713 plastic petri plate. Upon incubation at 32°C, cells adhere to the bottom of the plate and
714 undergo development. At the indicated times, developing populations were photographed
715 using a Leica Wild M8 microscope equipped with an Olympus E-620 digital camera.

716

717 ***Sample collection***

718 At the indicated times PS, the MC7 buffer overlay was replaced with 5 mL of fresh MC7 buffer
719 or 5 mL of MC7 buffer containing 50 μg/mL of rifampicin to inhibit transcription for
720 measurement of transcript degradation rates. Developing cells were scraped from the bottom
721 of the plates, the entire contents were collected in a 15-mL centrifuge tube, and samples were

722 mixed thoroughly as described previously (29). A 96-μL sample was removed, glutaraldehyde
723 was added, and the sample was stored as described above for the T_0 sample, fixing the cells for
724 quantification of total cells as described below. A 400 μL sample was removed and stored at -
725 20°C for measurement of sonication-resistant spores as described below. For the experiments
726 shown in Figures 8 and S4, a 100 μl sample was removed and added to an equal volume of 2×
727 sample buffer (0.125 M Tris-HCl [pH 6.8], 20% glycerol, 4% sodium dodecyl sulfate [SDS], 0.2%
728 bromophenol blue, 0.2 M dithiothreitol), boiled for 5 min, and stored at -20°C for immunoblot
729 analysis. Immediately after collecting the samples just described, the rest of the 1,000-Klett-
730 unit cell suspension was mixed with 0.5 mL of RNase stop solution (5% phenol [pH < 7] in
731 ethanol), followed by rapid cooling in liquid nitrogen until almost frozen, centrifugation at 8,700
732 × *g* for 10 min at 4°C, removal of the supernatant, freezing of the cell pellet in liquid nitrogen,
733 and storage at -80°C until RNA extraction.
734
735 ***Quantification of total cells, transitioning cells, and sonication-resistant spores***
736 The total number of cells, including rods, elliptical TCs, and round spores, was determined using
737 the glutaraldehyde-fixed samples collected as described above. Each sample was thawed and
738 mixed by vortexing and pipetting, diluted with MC7 buffer, sonicated for 10 s, and then all cells
739 were counted microscopically as described previously (29), except noting the number of cells
740 that were elliptical or round. The number of sonication-resistant spores in the 400-μL samples
741 collected as described above was quantified as described previously (38). These samples were
742 not glutaraldehyde-fixed and were sonicated for 10 s intervals three times with cooling on ice in
743 between, leaving only round spores (i.e., neither rods nor elliptical TCs were observed). The

744 total cell number minus the number of sonication-resistant spores was designated the number
745 of sonication-sensitive cells (consisting primarily of rods and a small percentage of TCs) and was
746 expressed as a percentage of the total cell number in the corresponding T_0 sample (consisting
747 only of rods). The number of cells that were elliptical or round in the glutaraldehyde-fixed
748 sample minus the number of sonication-resistant spores in the corresponding sample that was
749 not glutaraldehyde-fixed, was designated the number of TCs and was also expressed as a
750 percentage of the total cell number in the corresponding T_0 sample.
751
752 ***RNA extraction and analysis***
753 RNA was extracted using the hot-phenol method, followed by digestion with DNase I (Roche) as
754 described previously (36). The RNA (1 μg) was then subjected to cDNA synthesis using
755 Superscript III reverse transcriptase (InVitrogen) and random primers (Promega), as instructed
756 by the manufacturers. In parallel, RNA (1 μg) was subjected to cDNA synthesis reaction
757 conditions without Superscript III reverse transcriptase, as a control. One μl of cDNA at the
758 appropriate dilution (as determined empirically) and 20 pmol of each primer were subjected to
759 qPCR in a 25 μl reaction using 2× reaction buffer as described previously (29). qPCR was done
760 in quadruplicate for each cDNA using a LightCycler® 480 System (Roche). In parallel, a standard
761 curve was generated for each pair of qPCR primers using genomic DNA (gDNA) from *M. xanthus*
762 WT strain DK1622 and gene expression was quantified using the relative standard curve
763 method (user bulletin 2; Applied Biosystems). 16S rRNA was used as the internal standard for
764 each sample. The primers used for RT-qPCR analysis of 16S rRNA (93) and the late-acting
765 operons (39) have been described previously.

766 Relative transcript levels for mutants are the average of three biological replicates after
767 each replicate was normalized to the transcript level observed for one replicate of the WT
768 strain at the earliest time point (i.e., either 6 or 18 h PS) in the same experiment (29).
769 Transcript levels for the WT strain at other times PS were likewise normalized to that observed
770 for the WT strain at the earliest time point in the same experiment. For the WT strain at the
771 earliest time point, the transcript levels of at least three biological replicates from different
772 experiments were normalized to their average, which was set as 1.
773 To measure transcript degradation rates, samples were collected immediately after addition
774 of rifampicin (designated t_0) and 8 and 16 min later for RNA extraction and analysis as described
775 above. For each biological replicate the transcript levels after 8 and 16 min were normalized to
776 the transcript level at t_0, which was set as 1, and the natural log of the resulting values was
777 plotted versus minutes after rifampicin treatment (29). The slope of a linear fit of the data was
778 used to compute the mRNA half-life.
779
780 ***Expression and purification of proteins***
781 To express His-tagged proteins, *E. coli* strain BL21(DE3) was transformed with pET11a/FruA-
782 DBD-H_8, pET11km/FruA-H_6, or pPH158 (for H_6-MrpC) and transformants were selected on LB
783 1.5% agar containing 50 μg/mL ampicillin or kanamycin sulfate. In each case, a single colony
784 was used to inoculate 10 mL of LB supplemented with antibiotic, followed by overnight
785 incubation at 37°C with shaking. Five mL of overnight culture was used to inoculate 500 mL of
786 the same medium, followed by continued shaking at 37°C until the culture reached 60-80 Klett

787 units. IPTG (1 mM final concentration) was added to induce synthesis of the recombinant
788 protein. After 2 h, cells were harvested as reported previously (94) and stored at -80°C.
789 To purify His-tagged proteins, a modification of a protocol described previously (95) was
790 used. Each cell pellet was resuspended in 35 mL of lysis buffer (50 mM Na-phosphate buffer pH
791 8.0, 500 mM NaCl, 14 mM β-mercaptoethanol, protease inhibitors [1 Roche Mini EDTA-free
792 tablet/10 mL]). Cells were disrupted by sonication (4 times for 1 min with intermittent cooling
793 on ice). After centrifugation at 18,000 × *g* for 10 min at 4°C, the supernatant was mixed with 5
794 mL of lysis buffer containing 10% w/v Triton X-100, 1 mL of 1 M imidazole (pH 8.0), enough lysis
795 buffer for 50 mL total, and finally 0.5 mL of Ni-NTA agarose (Qiagen) that had been washed 3
796 times with lysis buffer containing 20 mM imidazole. The mixture was rotated for 1 h at 4°C.
797 The Ni-NTA agarose was collected by centrifugation at 700 × *g* for 3 min at 4°C and washed 4
798 times with 50 mL of lysis buffer containing 20 mM imidazole, 0.5% w/v Triton X-100, and 25%
799 w/v glycerol. The Ni-NTA agarose was rotated for 30 min at 4°C with 10 mL of elution buffer
800 (50 mM Na-phosphate buffer pH 8.0, 500 mM NaCl, 1.4 mM β-mercaptoethanol, protease
801 inhibitors [1 Roche Mini EDTA-free tablet], 250 mM imidazole, 0.5% w/v Triton X-100, 25% w/v
802 glycerol). Eluates were dialyzed twice at 4°C against 1 L of storage buffer (10 mM Tris-HCL pH
803 8.0, 100 mM NaCl, 1 mM β-mercaptoethanol, 10% w/v glycerol) and aliquots were stored at -
804 80°C. The protein concentration was determined using a Bradford (96) assay kit (Bio-Rad).
805 To express MBP-Nla6 DBD, *E. coli* strain BL21(DE3) was transformed with pMAL-c5x/MBP-
806 Nla6 DBD and transformants were selected on LB 1.5% agar containing 100 μg/mL ampicillin.
807 Five colonies were used to inoculate 80 mL of LB supplemented with antibiotic and 0.2%
808 dextrose, followed by incubation at 37°C with shaking at 350 rpm until the culture reached 60

809 Klett units. IPTG (0.3 mM final concentration) was added to induce synthesis of the
810 recombinant protein. After 2 h, cells were harvested, the cell pellet was resuspended in 10 mL
811 of column buffer (20 mM Tris-HCl pH 7.5, 200 mM NaCl, 1 mM EDTA, protease inhibitors [1
812 Roche Mini EDTA-free tablet], 10 mM β-mercaptoethanol), and the cell suspension was stored
813 at -20°C.

814 MBP-Nla6 DBD was purified according to instructions in the pMAL™ Protein Fusion &
815 Purification System manual (NEB). Briefly, the cell pellet was thawed and cells were disrupted
816 by sonication (8 times for 15 s with intermittent cooling on ice). After centrifugation at 18,000
817 × *g* for 20 min at 4°C, the supernatant was loaded onto a 1 mL amylose gravity-flow column,
818 which had been prewashed with 5 mL of column buffer. The loaded column was washed with
819 12 mL of column buffer, then eluted with 2.5 mL of column buffer supplemented with 10 mM
820 maltose, collecting fractions of 4 drops each (approximately 200 μL). Fractions were subjected
821 to SDS-PAGE with Coomassie Blue staining. Fractions 4-9, with maximal purified MBP-Nla6
822 DBD, were pooled, dialyzed as described above, and aliquots were stored at -80°C. The protein
823 concentration was determined by measuring the absorbance at 280 nm and using the
824 calculated extinction coefficient of MBP-Nla6 DBD (1.32 $[mg/mL]^{-1}cm^{-1}$).

825

826 ***Electrophoretic mobility shift assays***

827 ^{32}P-labelled DNA fragments were generated by PCR using primers labelled with [γ-^{32}P]ATP using
828 T4 polynucleotide kinase (NEB) according to the manufacturer's instructions. The templates for
829 PCR were either plasmid DNA or gDNA from *M. xanthus* WT strain DK1622. The primers and
830 templates were as follows: primers LK1298 and LK1331 with template pPV391 for *dev*, primers

831 *exoA-I* -171 fwd and *exoA-I* -1 rev with template gDNA for *exoA-I*, primers *fadIJ* -214 fwd and
832 *fadIJ* -5 rev with template gDNA for *fadIJ*, primers *exoL-P* -217 fwd and *exoL-P* +56 rev with
833 template gDNA for *exoL-P*, and primers *nfsA-H* -166 fwd and *nfsA-H* +35 with template pSS14
834 for *nfsA-H.* The labeled DNA fragments were purified by electrophoresis on 15%
835 polyacrylamide gels, followed by visualization using autoradiography, excision, and overnight
836 elution by soaking in TE buffer (10 mM Tris-HCl pH 8.0, 1 mM EDTA) as described previously
837 (94).
838 Binding reactions (10 μL) were performed as reported previously (94), except the reaction
839 mixtures were incubated at 37°C for 10 min prior to loading on 8% polyacrylamide gels. To
840 determine whether the order of protein addition was important, one protein was added to the
841 reaction mixture during an initial 10 min incubation at 37°C, followed by addition of a second
842 protein and another 10 min incubation at 37°C, prior to loading on 8% polyacrylamide gels.
843 Gels were dried and exposed to X-ray film for autoradiography as described (94).
844
845 **Acknowledgements**
846 We thank Monique Floer for advice about high-throughput qPCR and for use of the LightCycler®
847 480 System. We thank Anthony Garza, Lawrence Shimkets, Ramya Rajagopalan, Wenyuan Shi,
848 Sumiko Inouye, Montserrat Elias-Arnanz, and Penelope Higgs for sharing strains. We thank
849 Muqing Ma and Anthony Garza for constructing pMAL-c5x/MBP-ΔCNla6 DBD. This work was
850 supported by the National Science Foundation (awards MCB-1411272 and IOS-1951025) and by
851 salary support for L.K. from Michigan State University AgBioResearch.
852

853 **Author contributions**

854 Conception or design of the study: LK, SS

855 Acquisition of the data: SS, LK

856 Analysis or interpretation of the data: SS, LK

857 Writing of the manuscript: LK, SS

858

859 **References**

860 1. Yang Z, Higgs P, editors. Myxobacteria: genomics, cellular and molecular biology. Norfolk, UK:
861 Caister Academic Press; 2014.
862 2. O'Connor KA, Zusman DR. Behavior of peripheral rods and their role in the life cycle of *Myxococcus*
863 *xanthus*. J Bacteriol. 1991;173(11):3342-55.
864 3. Lee B, Holkenbrink C, Treuner-Lange A, Higgs PI. *Myxococcus xanthus* developmental cell fate
865 production: heterogeneous accumulation of developmental regulatory proteins and reexamination
866 of the role of MazF in developmental lysis. J Bacteriol. 2012;194(12):3058-68.
867 4. Munoz-Dorado J, Moraleda-Munoz A, Marcos-Torres FJ, Contreras-Moreno FJ, Martin-Cuadrado
868 AB, Schrader JM, et al. Transcriptome dynamics of the *Myxococcus xanthus* multicellular
869 developmental program. eLife. 2019;8:e50374.
870 5. Sharma G, Yao AI, Smaldone GT, Liang J, Long M, Facciotti MT, et al. Global gene expression
871 analysis of the *Myxococcus xanthus* developmental time course. Genomics. 2021;113(1 Pt 1):120-
872 34.
873 6. McLoon AL, Boeck ME, Bruckskotten M, Keyel AC, Sogaard-Andersen L. Transcriptomic analysis of
874 the *Myxococcus xanthus* FruA regulon, and comparative developmental transcriptomic analysis of
875 two fruiting body forming species, *Myxococcus xanthus* and *Myxococcus stipitatus*. BMC Genomics.
876 2021;22(1):784.
877 7. Kroos L. Highly signal-responsive gene regulatory network governing *Myxococcus* development.
878 Trends Genet. 2017;33:3-15.
879 8. Manoil C, Kaiser D. Accumulation of guanosine tetraphosphate and guanosine pentaphosphate in
880 *Myxococcus xanthus* during starvation and myxospore formation. J Bacteriol. 1980;141:297-304.
881 9. Harris BZ, Kaiser D, Singer M. The guanosine nucleotide (p)ppGpp initiates development and A-
882 factor production in *Myxococcus xanthus*. Genes Dev. 1998;12(7):1022-35.
883 10. Skotnicka D, Smaldone GT, Petters T, Trampari E, Liang J, Kaever V, et al. A minimal threshold of c-
884 di-GMP is essential for fruiting body formation and sporulation in *Myxococcus xanthus*. PLoS Genet.
885 2016;12(5):e1006080.
886 11. Singer M, Kaiser D. Ectopic production of guanosine penta-and tetraphosphate can initiate early
887 developmental gene expression in *Myxococcus xanthus*. Genes and Dev. 1995;9:1633-44.
888 12. Crawford EW, Jr., Shimkets LJ. The *Myxococcus xanthus socE* and *csgA* genes are regulated by the
889 stringent response. Mol Microbiol. 2000;37(4):788-99.

890 13. Konovalova A, Lobach S, Sogaard-Andersen L. A RelA-dependent two-tiered regulated proteolysis
891 cascade controls synthesis of a contact-dependent intercellular signal in *Myxococcus xanthus*. Mol
892 Microbiol. 2012;84(2):260-75.
893 14. Konovalova A, Wegener-Feldbrugge S, Sogaard-Andersen L. Two intercellular signals required for
894 fruiting body formation in *Myxococcus xanthus* act sequentially but non-hierarchically. Mol
895 Microbiol. 2012;86(1):65-81.
896 15. Bretl DJ, Kirby JR. Molecular mechanisms of signaling in *Myxococcus xanthus* development. J Mol
897 Biol. 2016;428:3805-30.
898 16. Kuspa A, Kroos L, Kaiser D. Intercellular signaling is required for developmental gene expression in
899 *Myxococcus xanthus*. Dev Biol. 1986;117:267-76.
900 17. Kroos L, Kaiser D. Expression of many developmentally regulated genes in *Myxococcus* depends on
901 a sequence of cell interactions. Genes Dev. 1987;1:840-54.
902 18. Kim SK, Kaiser D. Cell motility is required for the transmission of C-factor, an intercellular signal that
903 coordinates fruiting body morphogenesis of *Myxococcus xanthus*. Genes Dev. 1990;4:896-905.
904 19. Kim SK, Kaiser D. Cell alignment required in differentiation of *Myxococcus xanthus*. Science.
905 1990;249:926-8.
906 20. Kroos L, Hartzell P, Stephens K, Kaiser D. A link between cell movement and gene expression argues
907 that motility is required for cell-cell signaling during fruiting body development. Genes Dev.
908 1988;2:1677-85.
909 21. Kim SK, Kaiser D. C-factor has distinct aggregation and sporulation thresholds during *Myxococcus*
910 development. J Bacteriol. 1991;173:1722-8.
911 22. Kruse T, Lobedanz S, Berthelsen NM, Sogaard-Andersen L. C-signal: a cell surface-associated
912 morphogen that induces and co-ordinates multicellular fruiting body morphogenesis and
913 sporulation in *Myxococcus xanthus*. Mol Microbiol. 2001;40(1):156-68.
914 23. Li S-F, Lee B, Shimkets LJ. *csgA* expression entrains *Myxococcus xanthus* development. Genes Dev.
915 1992;6:401-10.
916 24. Kim SK, Kaiser D. C-factor: a cell-cell signaling protein required for fruiting body morphogenesis of
917 *M. xanthus*. Cell. 1990;61:19-26.
918 25. Lobedanz S, Sogaard-Andersen L. Identification of the C-signal, a contact-dependent morphogen
919 coordinating multiple developmental responses in *Myxococcus xanthus*. Genes Dev.
920 2003;17(17):2151-61.
921 26. Rolbetzki A, Ammon M, Jakovljevic V, Konovalova A, Sogaard-Andersen L. Regulated secretion of a
922 protease activates intercellular signaling during fruiting body formation in *M. xanthus*. Dev Cell.
923 2008;15(4):627-34.
924 27. Boynton TO, Shimkets LJ. *Myxococcus* CsgA, *Drosophila* Sniffer and human HSD17B10 are
925 cardiolipin phospholipases. Genes Dev. 2015;29:1903-14.
926 28. Ellehauge E, Norregaard-Madsen M, Sogaard-Andersen L. The FruA signal transduction protein
927 provides a checkpoint for the temporal co-ordination of intercellular signals in *Myxococcus xanthus*
928 development. Mol Microbiol. 1998;30:807-17.
929 29. Saha S, Patra P, Igoshin O, Kroos L. Systematic analysis of the *Myxococcus xanthus* developmental
930 gene regulatory network supports posttranslational regulation of FruA by C-signaling. Mol
931 Microbiol. 2019;111:1732-52.
932 30. Ogawa M, Fujitani S, Mao X, Inouye S, Komano T. FruA, a putative transcription factor essential for
933 the development of *Myxococcus xanthus*. Mol Microbiol. 1996;22(4):757-67.
934 31. Mittal S, Kroos L. A combination of unusual transcription factors binds cooperatively to control
935 *Myxococcus xanthus* developmental gene expression. Proc Natl Acad Sci USA. 2009;106:1965-70.

936 32. Giglio KM, Caberoy N, Suen G, Kaiser D, Garza AG. A cascade of coregulating enhancer binding
937 proteins initiates and propagates a multicellular developmental program. Proc Natl Acad Sci USA.
938 2011;108:E431-E9.
939 33. Ueki T, Inouye S. Identification of an activator protein required for the induction of *fruA*, a gene
940 essential for fruiting body development in *Myxococcus xanthus*. Proc Natl Acad Sci USA.
941 2003;100(15):8782-7.
942 34. Nariya H, Inouye S. A protein Ser/Thr kinase cascade negatively regulates the DNA-binding activity
943 of MrpC, a smaller form of which may be necessary for the *Myxococcus xanthus* development. Mol
944 Microbiol. 2006;60(5):1205-17.
945 35. McLaughlin PT, Bhardwaj V, Feeley BE, Higgs PI. MrpC, a CRP/Fnr homolog, functions as a negative
946 autoregulator during the *Myxococcus xanthus* multicellular developmental program. Mol Microbiol.
947 2018;109:245-61.
948 36. Higgs PI, Jagadeesan S, Mann P, Zusman DR. EspA, an orphan hybrid histidine protein kinase,
949 regulates the timing of expression of key developmental proteins of *Myxococcus xanthus*. J
950 Bacteriol. 2008;190:4416-26.
951 37. Schramm A, Lee B, Higgs PI. Intra- and inter-protein phosphorylation between two hybrid histidine
952 kinases controls *Myxococcus xanthus* developmental progression. J Biol Chem. 2012;287:25060–72.
953 38. Rajagopalan R, Kroos L. Nutrient-regulated proteolysis of MrpC halts expression of genes important
954 for commitment to sporulation during *Myxococcus xanthus* development. J Bacteriol.
955 2014;196:2736-47.
956 39. Hoang Y, Kroos L. Ultrasensitive response of developing *Myxococcus xanthus* to the addition of
957 nutrient medium correlates with the level of MrpC. J Bacteriol. 2018;200:e00456-18.
958 40. Feeley BE, Bhardwaj V, McLaughlin PT, Diggs S, Blaha GM, Higgs PI. An amino-terminal
959 threonine/serine motif is necessary for activity of the Crp/Fnr homolog, MrpC and for *Myxococcus*
960 *xanthus* developmental robustness. Mol Microbiol. 2019;112(5):1531-51.
961 41. Robinson M, Son B, Kroos L. Transcription factor MrpC binds to promoter regions of many
962 developmentally-regulated genes in *Myxococcus xanthus*. BMC Genomics. 2014;15:1123.
963 42. Campbell A, Viswanathan P, Barrett T, Son B, Saha S, Kroos L. Combinatorial regulation of the *dev*
964 operon by MrpC2 and FruA during *Myxococcus xanthus* development. J Bacteriol. 2015;197:240-51.
965 43. Lee J, Son B, Viswanathan P, Luethy P, Kroos L. Combinatorial regulation of *fmgD* by MrpC2 and
966 FruA during *Myxococcus xanthus* development. J Bacteriol. 2011;193:1681-9.
967 44. Mittal S, Kroos L. Combinatorial regulation by a novel arrangement of FruA and MrpC2
968 transcription factors during *Myxococcus xanthus* development. J Bacteriol. 2009;191:2753-63.
969 45. Son B, Liu Y, Kroos L. Combinatorial regulation by MrpC2 and FruA involves three sites in the *fmgE*
970 promoter region during *Myxococcus xanthus* development. J Bacteriol. 2011;193:2756-66.
971 46. Hoang Y, Franklin JL, Dufour YS, Kroos L. Cell density, alignment, and orientation correlate with C-
972 signal-dependent gene expression during *Myxococcus xanthus* development. Proc Natl Acad Sci
973 USA. 2021;118(45):e2111706118.
974 47. Kroos L, Kuspa A, Kaiser D. A global analysis of developmentally regulated genes in *Myxococcus*
975 *xanthus*. Dev Biol. 1986;117:252-66.
976 48. Kroos L, Kuspa A, Kaiser D. Defects in fruiting body development caused by Tn*5 lac* insertions in
977 *Myxococcus xanthus*. J Bacteriol. 1990;172:484-7.
978 49. Boysen A, Ellehauge E, Julien B, Sogaard-Andersen L. The DevT protein stimulates synthesis of FruA,
979 a signal transduction protein required for fruiting body morphogenesis in *Myxococcus xanthus*. J
980 Bacteriol. 2002;184(6):1540-6.
981 50. Thony-Meyer L, Kaiser D. *devRS*, an autoregulated and essential genetic locus for fruiting body
982 development in *Myxococcus xanthus*. J Bacteriol. 1993;175:7450-62.

983 51. Viswanathan P, Murphy K, Julien B, Garza AG, Kroos L. Regulation of *dev*, an operon that includes
984 genes essential for *Myxococcus xanthus* development and CRISPR-associated genes and repeats. J
985 Bacteriol. 2007;189:3738-50.
986 52. Rajagopalan R, Wielgoss S, Lippert G, Velicer GJ, Kroos L. *devI* is an evolutionarily young negative
987 regulator of *Myxococcus xanthus* development. J Bacteriol. 2015;197(7):1249-62.
988 53. Rajagopalan R, Kroos L. The *dev* operon regulates the timing of sporulation during *Myxococcus*
989 *xanthus* development. J Bacteriol. 2017;199(10):e00788-16.
990 54. Makarova KS, Aravind L, Wolf YI, Koonin EV. Unification of Cas protein families and a simple
991 scenario for the origin and evolution of CRISPR-Cas systems. Biol Direct. 2011;6:38.
992 55. Bullock HA, Shen H, Boynton TO, Shimkets LJ. Fatty acid oxidation is required for *Myxococcus*
993 *xanthus* development. J Bacteriol. 2018;200(10):e00572-17.
994 56. Kuzmich S, Blumenkamp P, Meier D, Szadkowski D, Goesmann A, Becker A, et al. CRP-Like
995 transcriptional regulator MrpC curbs c-di-GMP and 3',3'-cGAMP nucleotide levels during
996 development in *Myxococcus xanthus*. mBio. 2022;13:e00044-22.
997 57. Muller FD, Treuner-Lange A, Heider J, Huntley SM, Higgs PI. Global transcriptome analysis of spore
998 formation in *Myxococcus xanthus* reveals a locus necessary for cell differentiation. BMC Genomics.
999 2010;11:264.
1000 58. Muller FD, Schink CW, Hoiczyk E, Cserti E, Higgs PI. Spore formation in *Myxococcus xanthus* is tied
1001 to cytoskeleton functions and polysaccharide spore coat deposition. Mol Microbiol.
1002 2012;83(3):486-505.
1003 59. Holkenbrink C, Hoiczyk E, Kahnt J, Higgs PI. Synthesis and assembly of a novel glycan layer in
1004 *Myxococcus xanthus* spores. J Biol Chem. 2014;289(46):32364-78.
1005 60. Wartel M, Ducret A, Thutupalli S, Czerwinski F, Le Gall AV, Mauriello EM, et al. A versatile class of
1006 cell surface directional motors gives rise to gliding motility and sporulation in *Myxococcus xanthus*.
1007 PLoS Biol. 2013;11(12):e1001728.
1008 61. Licking E, Gorski L, Kaiser D. A common step for changing cell shape in fruiting body and starvation-
1009 independent sporulation of *Myxococcus xanthus*. J Bacteriol. 2000;182(12):3553-8.
1010 62. Ueki T, Inouye S. Identification of a gene involved in polysaccharide export as a transcription target
1011 of FruA, an essential factor for *Myxococcus xanthus* development. J Biol Chem.
1012 2005;280(37):32279-84.
1013 63. Giglio KM, Zhu C, Klunder C, Kummer S, Garza AG. The enhancer binding protein Nla6 regulates
1014 developmental genes that are important for *Myxococcus xanthus* sporulation. J Bacteriol.
1015 2015;197(7):1276-87.
1016 64. Perez-Burgos M, Garcia-Romero I, Valvano MA, Sogaard Andersen L. Identification of the Wzx
1017 flippase, Wzy polymerase and sugar-modifying enzymes for spore coat polysaccharide biosynthesis
1018 in *Myxococcus xanthus*. Mol Microbiol. 2020;113(6):1189-208.
1019 65. Kaiser D. Social gliding is correlated with the presence of pili in *Myxococcus xanthus*. Proc Natl Acad
1020 Sci USA. 1979;76:5952-6.
1021 66. Caberoy NB, Welch RD, Jakobsen JS, Slater SC, Garza AG. Global mutational analysis of NtrC-like
1022 activators in *Myxococcus xanthus*: identifying activator mutants defective for motility and fruiting
1023 body development. J Bacteriol. 2003;185(20):6083-94.
1024 67. Davidson EH. Genomic Regulatory Systems. San Diego: Academic Press; 2001.
1025 68. Rickels R, Shilatifard A. Enhancer logic and mechanics in development and disease. Trends Cell Biol.
1026 2018;28(8):608-30.
1027 69. Panigrahi A, O'Malley BW. Mechanisms of enhancer action: the known and the unknown. Genome
1028 Biol. 2021;22(1):108.
1029 70. Mohanraju P, Saha C, van Baarlen P, Louwen R, Staals RHJ, van der Oost J. Alternative functions of
1030 CRISPR-Cas systems in the evolutionary arms race. Nat Rev Microbiol. 2022;20(6):351-64.

1031 71. Koonin EV, Makarova KS. Evolutionary plasticity and functional versatility of CRISPR systems. PLoS
1032 Biol. 2022;20(1):e3001481.
1033 72. Munoz-Dorado J, Inouye S, Inouye M. A gene encoding a protein serine/threonine kinase is
1034 required for normal development of *M. xanthus*, a Gram-negative bacterium. Cell. 1991;67:995-
1035 1006.
1036 73. Kroos L. Eukaryotic-like signaling and gene regulation in a prokaryote that undergoes multicellular
1037 development. Proc Natl Acad Sci USA. 2005;102(8):2681-2.
1038 74. Rajagopalan R, Sarwar Z, Garza AG, Kroos L. Developmental gene regulation. In: Yang Z, Higgs P,
1039 editors. Myxobacteria: genomics, cellular and molecular biology. Norfolk, UK: Caister Academic
1040 Press; 2014. p. 105-26.
1041 75. Sun H, Shi W. Genetic studies of *mrp*, a locus essential for cellular aggregation and sporulation of
1042 *Myxococcus xanthus*. J Bacteriol. 2001;183(16):4786-95.
1043 76. Wireman JW. Developmental induction of *Myxococcus xanthus* myxospores. J Bacteriol.
1044 1979;140:147-63.
1045 77. Kroos L. Bacterial development in the fast lane. J Bacteriol. 2008;190:4373-6.
1046 78. Bressuire-Isoard C, Broussolle V, Carlin F. Sporulation environment influences spore properties in
1047 *Bacillus*: evidence and insights on underlying molecular and physiological mechanisms. FEMS
1048 Microbiol Rev. 2018;42(5):614-26.
1049 79. Isticato R, Lanzilli M, Petrillo C, Donadio G, Baccigalupi L, Ricca E. *Bacillus subtilis* builds structurally
1050 and functionally different spores in response to the temperature of growth. Environ Microbiol.
1051 2020;22(1):170-82.
1052 80. Hamiot A, Lemy C, Krzewinski F, Faille C, Dubois T. Sporulation conditions influence the surface and
1053 adhesion properties of *Bacillus subtilis* spores. Front Microbiol. 2023;14:1219581.
1054 81. Eichenberger P, Fujita M, Jensen ST, Conlon EM, Rudner DZ, Wang ST, et al. The program of gene
1055 transcription for a single differentiating cell type during sporulation in *Bacillus subtilis*. PLoS Biol.
1056 2004;2(10):1664-83.
1057 82. Kroos L. The *Bacillus* and *Myxococcus* developmental networks and their transcriptional regulators.
1058 Ann Rev Genet. 2007;41:13-39.
1059 83. Arrieta-Ortiz ML, Hafemeister C, Bate AR, Chu T, Greenfield A, Shuster B, et al. An experimentally
1060 supported model of the *Bacillus subtilis* global transcriptional regulatory network. Mol Syst Biol.
1061 2015;11(11):839.
1062 84. McKenney PT, Driks A, Eichenberger P. The *Bacillus subtilis* endospore: assembly and functions of
1063 the multilayered coat. Nat Rev Microbiol. 2013;11(1):33-44.
1064 85. Shuster B, Khemmani M, Abe K, Huang X, Nakaya Y, Maryn N, et al. Contributions of crust proteins
1065 to spore surface properties in *Bacillus subtilis*. Mol Microbiol. 2019;111(3):825-43.
1066 86. Shuster B, Khemmani M, Nakaya Y, Holland G, Iwamoto K, Abe K, et al. Expansion of the spore
1067 surface polysaccharide layer in *Bacillus subtilis* by deletion of genes encoding glycosyltransferases
1068 and glucose modification enzymes. J Bacteriol. 2019;201(19):e00321-19.
1069 87. La Fortezza M, Rendueles O, Keller H, Velicer GJ. Hidden paths to endless forms most wonderful:
1070 ecology latently shapes evolution of multicellular development in predatory bacteria. Commun
1071 Biol. 2022;5(1):977.
1072 88. Kalathera J, Patel V, Pande S. Differential evolution of cooperative traits in aggregative multicellular
1073 bacterium *Myxococcus xanthus* driven by varied population bottleneck sizes. bioRxiv. 2023;doi:
1074 https://doi.org/10.1101/2023.09.20.558552.
1075 89. Kashefi K, Hartzell P. Genetic supression and phenotypic masking of a *Myxococcus xanthux frzF*$^{-}$
1076 defect. Molec Microbiol. 1995;15:483-94.

1077 90. Iniesta AA, Garcia-Heras F, Abellon-Ruiz J, Gallego-Garcia A, Elias-Arnanz M. Two systems for
1078 conditional gene expression in *Myxococcus xanthus* inducible by isopropyl-β-D-
1079 thiogalactopyranoside or vanillate. J Bacteriol. 2012;194(21):5875-85.
1080 91. Gibson DG, Young L, Chuang RY, Venter JC, Hutchison CA, 3rd, Smith HO. Enzymatic assembly of
1081 DNA molecules up to several hundred kilobases. Nat Methods. 2009;6(5):343-5.
1082 92. Sambrook J, Fritsch E, Maniatis T. Molecular Cloning: a laboratory manual, 2nd ed. Cold Spring
1083 Harbor: Cold Spring Harbor Laboratory Press; 1989.
1084 93. Ossa F, Diodati ME, Caberoy NB, Giglio KM, Edmonds M, Singer M, et al. The *Myxococcus xanthus*
1085 Nla4 protein is important for expression of stringent response-associated genes, ppGpp
1086 accumulation, and fruiting body development. J Bacteriol. 2007;189(23):8474-83.
1087 94. Yoder-Himes D, Kroos L. Regulation of the *Myxococcus xanthus* C-signal-dependent Ω4400
1088 promoter by the essential developmental protein FruA. J Bacteriol. 2006;188:5167-76.
1089 95. Nariya H, Inouye S. Identification of a protein Ser/Thr kinase cascade that regulates essential
1090 transcriptional activators in *Myxococcus xanthus* development. Mol Microbiol. 2005;58(2):367-79.
1091 96. Bradford M. A rapid and sensitive method for the quantitation of microgram quantities of protein
1092 utilizing the principle of protein-dye binding. Anal Biochem. 1976;72:248-54.
1093 97. Sun H, Shi W. Analyses of *mrp* genes during *Myxococcus xanthus* development. J Bacteriol.
1094 2001;183(23):6733-9.
1095 98. Viswanathan P, Ueki T, Inouye S, Kroos L. Combinatorial regulation of genes essential for
1096 *Myxococcus xanthus* development involves a response regulator and a LysR-type regulator. Proc
1097 Natl Acad Sci USA. 2007;104:7969-74.

1098

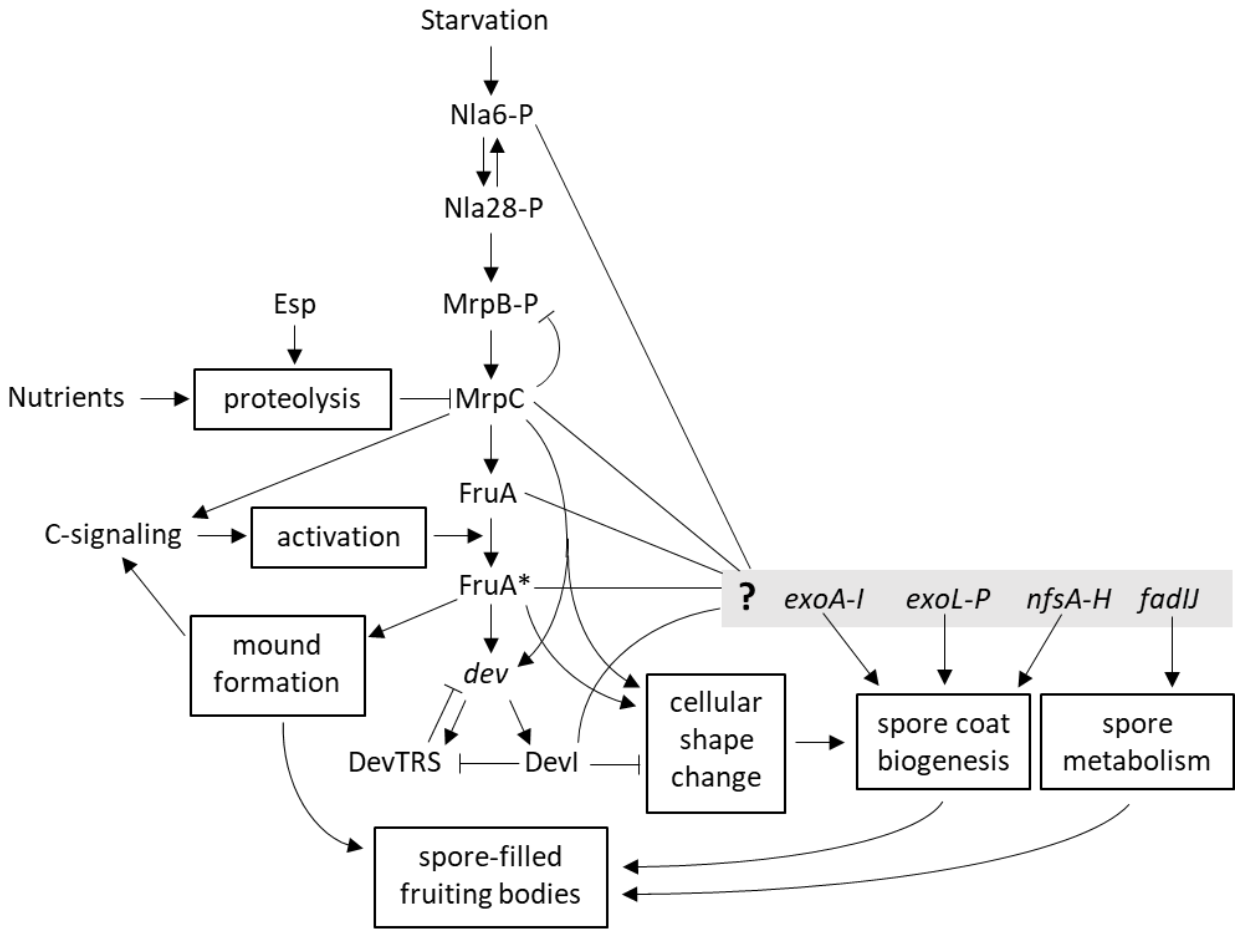

Figure 1. Model of the gene regulatory network governing formation of *M. xanthus* fruiting bodies. Starvation increases the level of phosphorylated Nla6 (Nla6-P), Nla28-P, MrpB-P, and MrpC in a cascade of transcription factors (7, 32, 35). Nutrients (38, 39) and Esp signaling (36, 37) can negatively regulate MrpC *via* proteolysis, and MrpC negatively autoregulates by competing with MrpB-P for binding to the *mrpC* promoter region (35). MrpC positively regulates C-signaling (97) and *fruA* transcription (33), leading to production of unactivated FruA. C-signaling activates FruA to FruA* by an unknown mechanism (28, 29). FruA* positively regulates mound formation (30), which enhances C-signaling (18-20), forming a positive feedback loop. FruA* also positively regulates the *dev* operon (98) together with MrpC (42), thus forming a feed-forward loop that has been speculated to also increase transcription of genes involved in cellular shape change (29). DevTRS proteins negatively autoregulate, decreasing DevI, which negatively regulates cellular shape change (52, 53) and may inhibit negative autoregulation by DevTRS (29). Here, we investigate possible regulation by Nla6-P, MrpC, FruA or FruA*, and DevI (lines to gray box with **?**) of late-acting operons involved in spore metabolism and spore coat biogenesis.

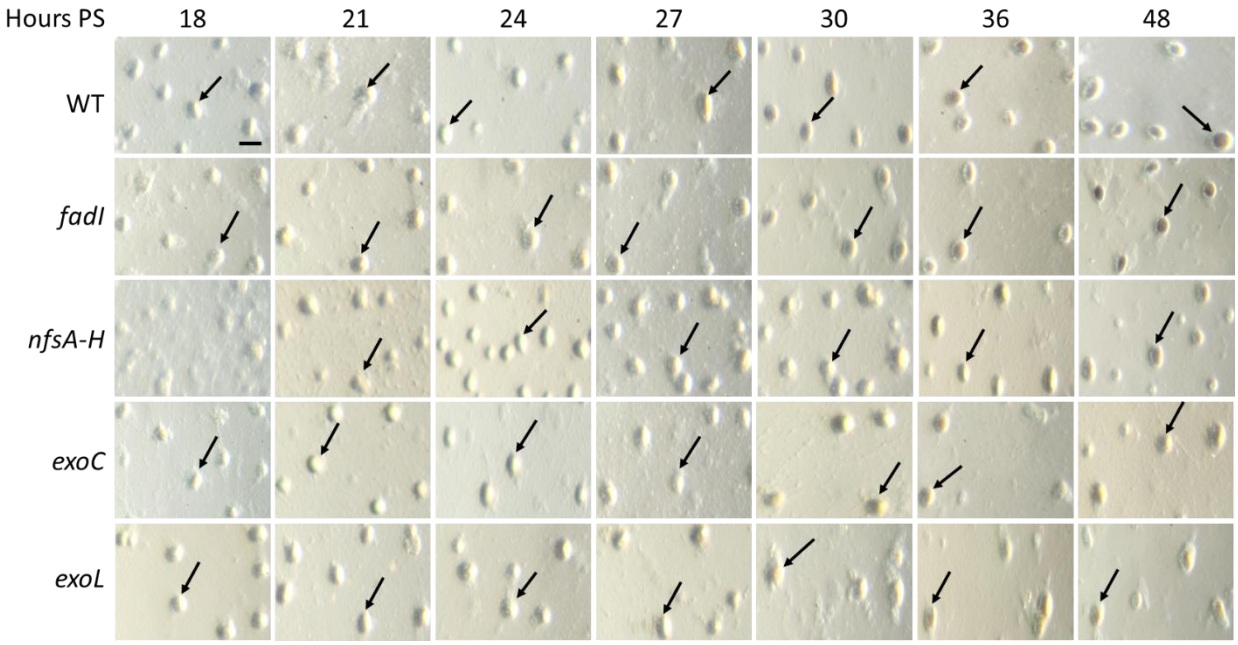

1116
1117
1118 Figure 2. Development of *M. xanthus* strains. The WT strain and its indicated mutant
1119 derivatives were subjected to starvation under submerged culture condition and microscopic
1120 images were obtained at the indicated times PS. The WT strain and all the mutants except
1121 *nfsA-H* formed compact mounds by 18 h (an arrow points to one in each panel). The *nfsA-H*
1122 mutant formed compact mounds by 21 h. Mounds of the WT strain began to darken by 30 h.
1123 Mounds of the *nfsA-H*, *exoC*, and *exoL* mutants darkened by 30 h but remained slightly less dark
1124 than mounds of the WT strain and the *fadI* mutant by 48 h. Bar, 100 μm. Similar results were
1125 observed in at least three biological replicates.
1126

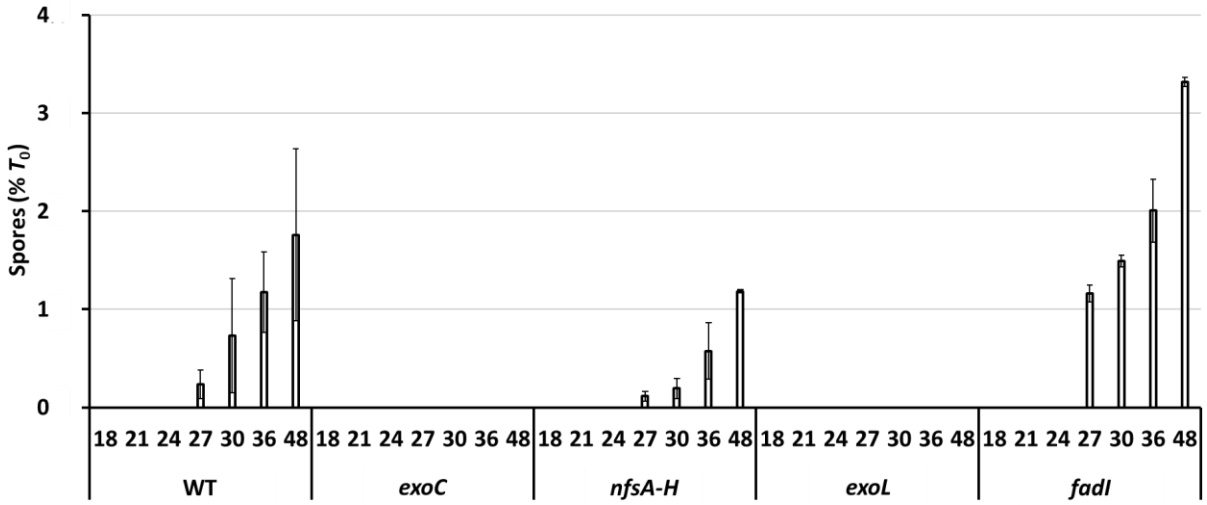

1127
1128
1129 Figure 3. Sonication-resistant spores during *M. xanthus* development. The WT strain and its
1130 indicated mutant derivatives were subjected to starvation under submerged culture conditions.
1131 Samples were collected at the indicated times PS for quantification of sonication-resistant
1132 spores. Values are expressed as a percentage of the number of rod-shaped cells present at the
1133 time starvation initiated development (T_0) (Table S1). Bars show the average of three biological
1134 replicates and error bars indicate one standard deviation.
1135

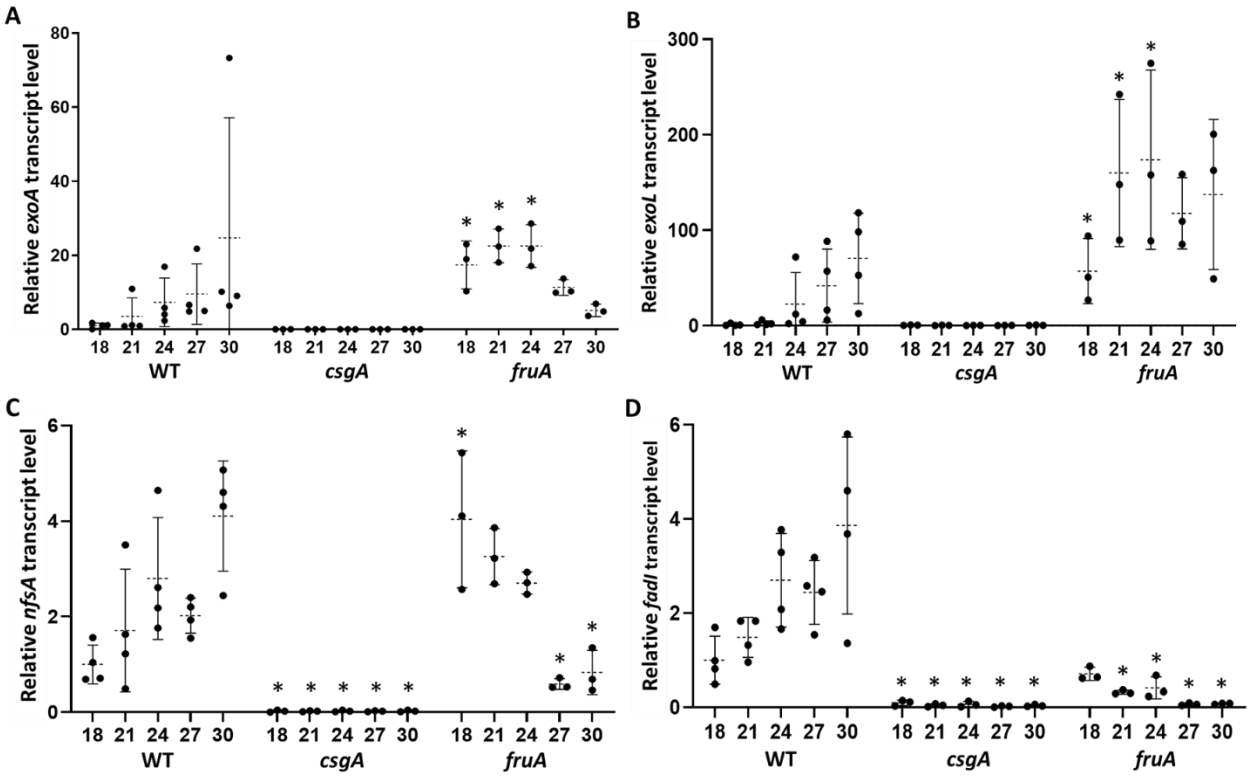

Figure 4. Transcript levels in the WT strain and the *csgA* and *fruA* mutants late in *M. xanthus* development. The WT strain and its mutant derivatives were subjected to starvation under submerged culture conditions. Samples were collected at the indicated times PS for measurement of the *exoA* (A), *exoL* (B), *nfsA* (C), and *fadI* (D) transcript levels by RT-qPCR. Graphs show the data points and the average of at least three biological replicates, relative to the WT strain at 18 h PS, and error bars indicate one standard deviation. Asterisks indicate a difference ($p < 0.05$ in Student's two-tailed *t*-tests) from the WT strain at the corresponding time PS.

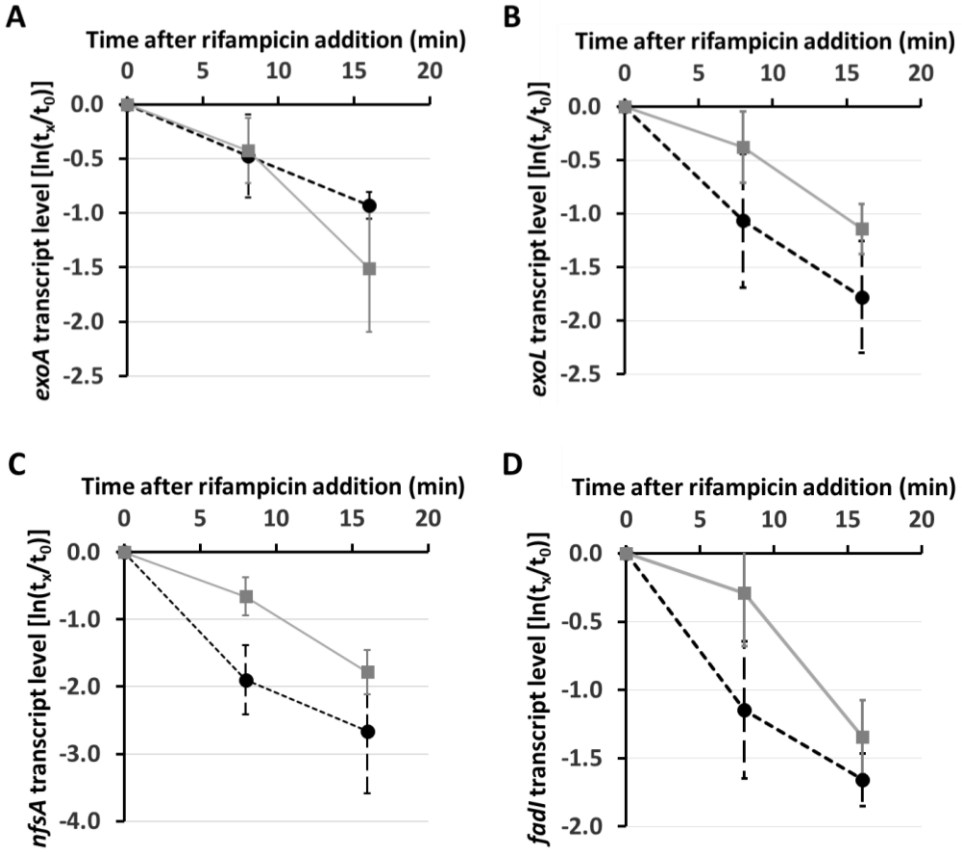

E

Transcript	Half-life in the WT strain (min)	Half-life in the *csgA* mutant (min)	*p* value
exoA	12 ± 2	8 ± 3	$p = 0.13$
exoL	8 ± 3	10 ± 2	$p = 0.20$
nfsA	5 ± 2	7 ± 1	$p = 0.26$
fadI	7 ± 1	9 ± 2	$p = 0.26$

Figure 5. Transcript stability in the WT strain and the *csgA* mutant late in *M. xanthus* development. The WT strain and the *csgA* mutant were subjected to starvation under submerged culture conditions for 30 h. The overlay was replaced with fresh starvation buffer containing rifampicin (50 μg/mL) and samples were collected immediately (t_0) and at the indicated times (t_x) for measurement of the *exoA* (A), *exoL* (B), *nfsA* (C), and *fadI* (D) transcript levels by RT-qPCR. Transcript levels at t_x were normalized to that at t_0 for each of three biological replicates and used to determine the transcript half-life for each replicate. The graph shows the average $\ln(t_x/t_0)$ and one standard deviation for the three biological replicates of the WT strain (black dashed line) and the *csgA* mutant (gray solid line). The average half-life and one standard deviation, as well as the *p* value from a Student's two-tailed *t*-test, are reported in (E).

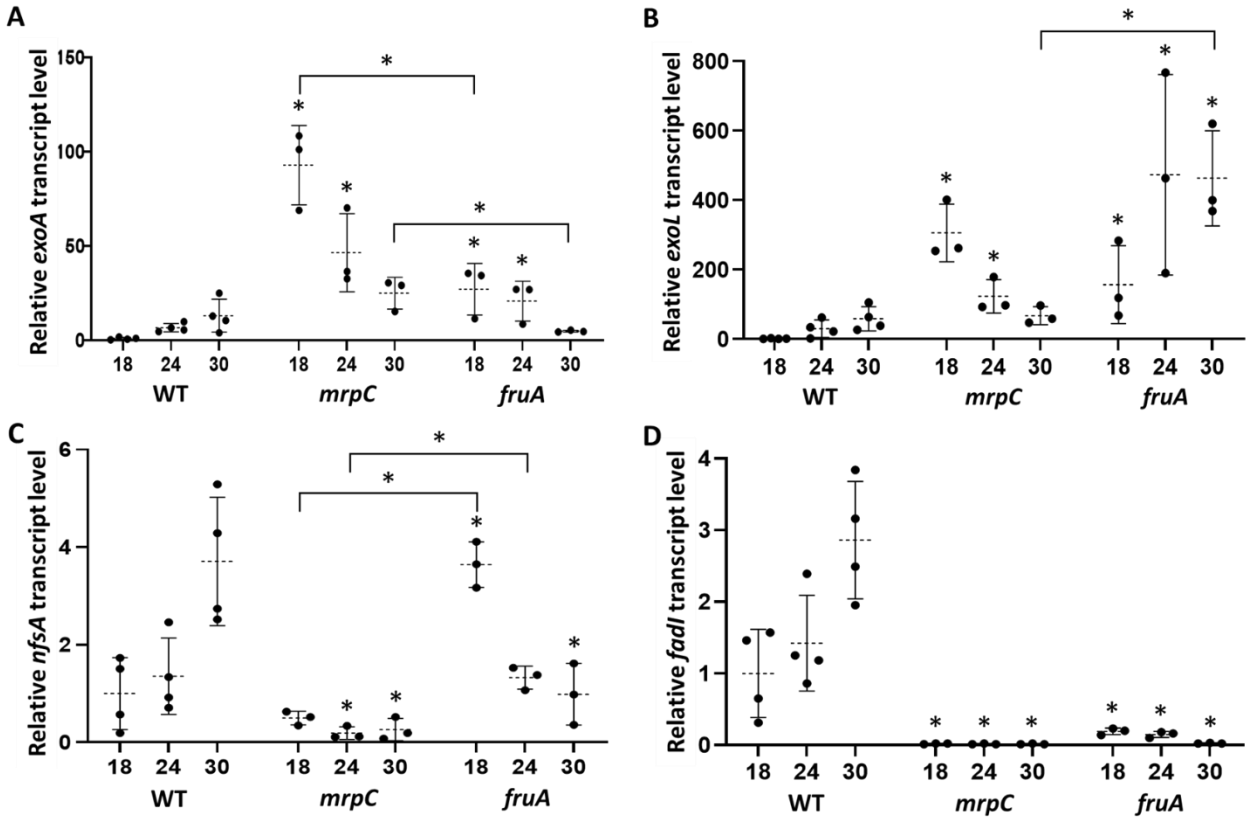

Figure 6. Transcript levels in the WT strain and the *mrpC* and *fruA* mutants late in *M. xanthus* development. The WT strain and its mutant derivatives were subjected to starvation under submerged culture conditions. Samples were collected at the indicated times PS for measurement of *exoA* (A), *exoL* (B), *nfsA* (C), and *fadI* (D) transcript levels by RT-qPCR. Graphs show the data points and the average of at least three biological replicates, relative to the WT strain at 18 h PS, and error bars indicate one standard deviation. Asterisks above error bars indicate a difference ($p < 0.05$ in Student's two-tailed *t*-tests) from the WT strain at the corresponding time PS and asterisks above brackets indicate a difference between the mutants.

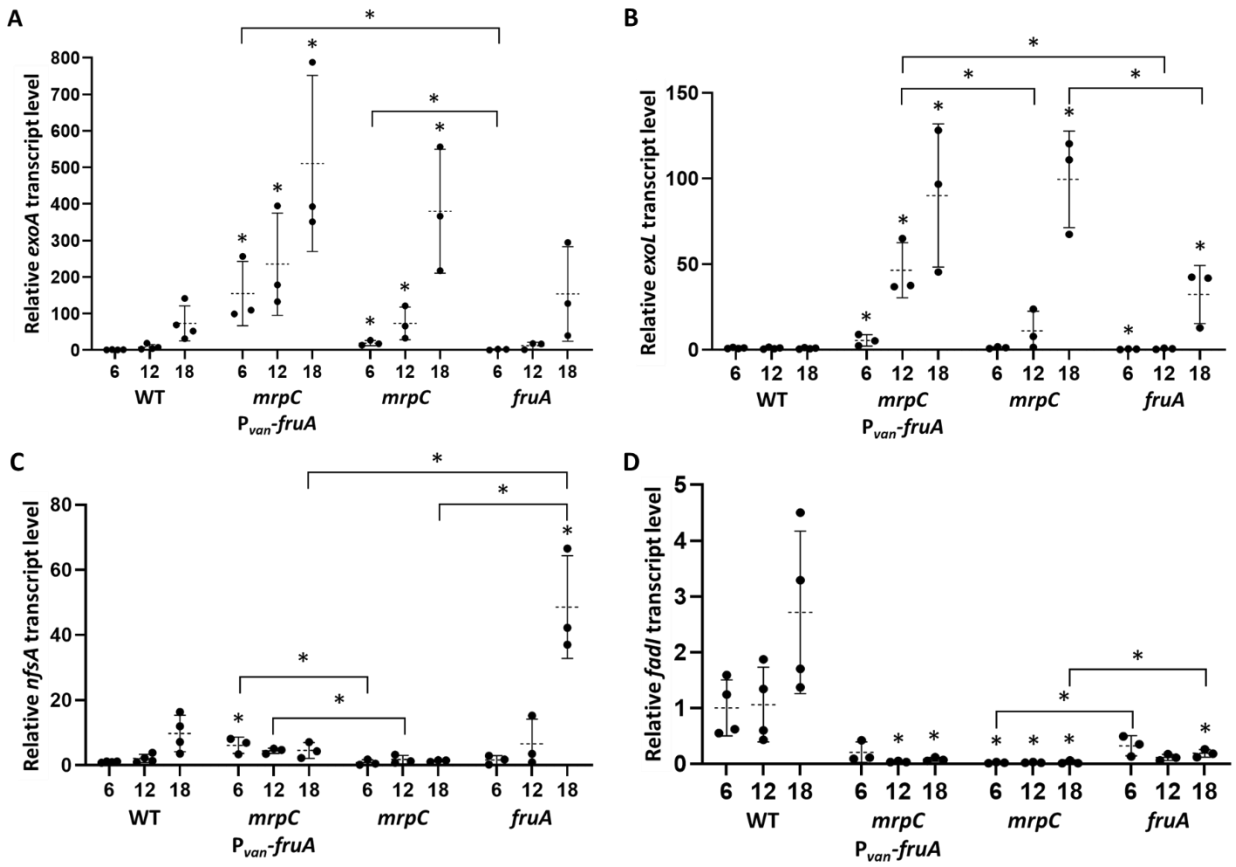

Figure 7. Transcript levels in the WT strain, the *mrpC* mutant with inducible *fruA*, and the *mrpC* and *fruA* mutants early in *M. xanthus* development. The WT strain and its mutant derivatives were subjected to starvation under submerged culture conditions. Samples were collected at the indicated times PS for measurement of *exoA* (A), *exoL* (B), *nfsA* (C), and *fadI* (D) transcript levels by RT-qPCR. Expression of *fruA* fused to P_{van} was induced with vanillate (0.5 mM) during growth and at 0 h PS. Graphs show the data points and the average of at least three biological replicates, relative to the WT strain at 6 h PS, and error bars indicate one standard deviation. Asterisks above error bars indicate a difference ($p < 0.05$ in Student's two-tailed *t*-tests) from the WT strain at the corresponding time PS and asterisks above brackets indicate a difference between the mutants.

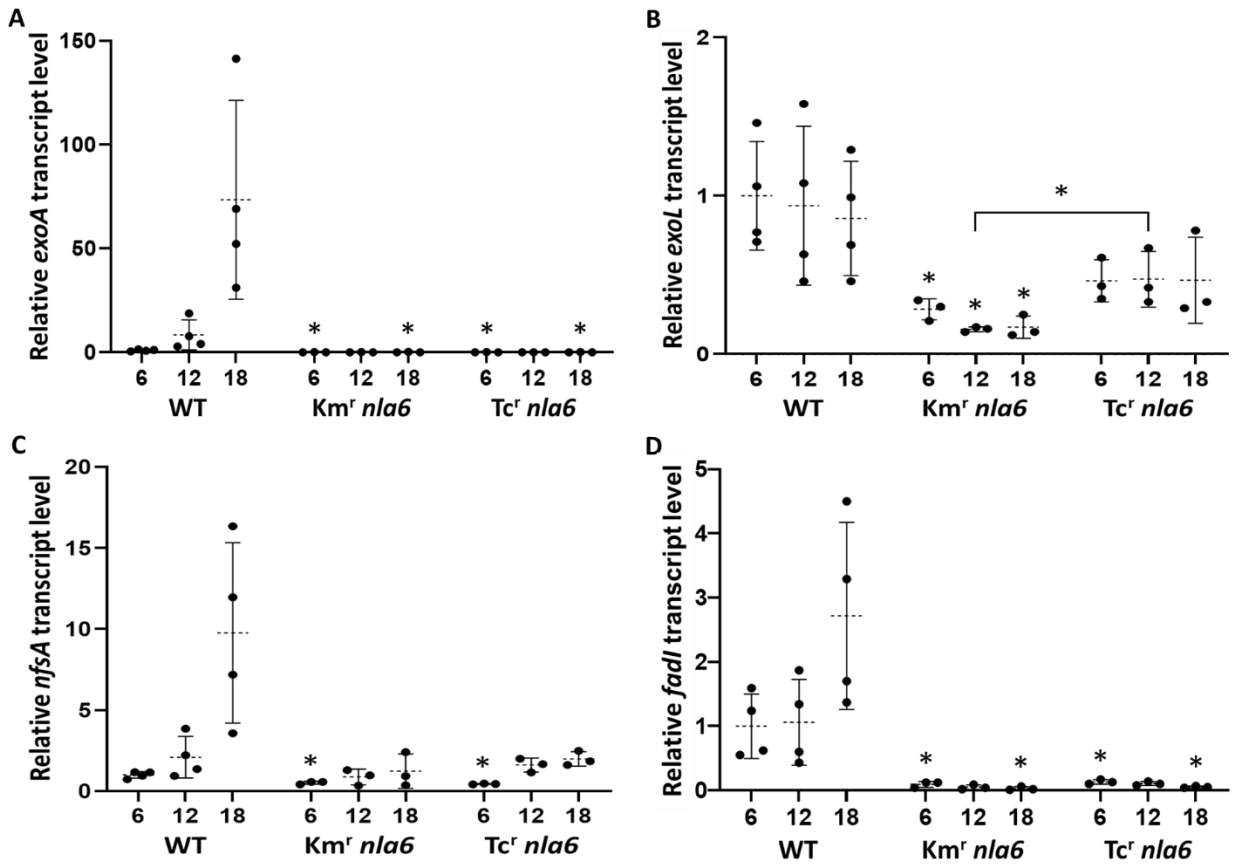

Figure 8. Transcript levels in *nla6* mutants early in *M. xanthus* development. The WT strain and its mutant derivatives were subjected to starvation under submerged culture conditions. Samples were collected at the indicated times PS for measurement of *exoA* (A), *exoL* (B), *nfsA* (C), and *fadI* (D) transcript levels by RT-qPCR. Graphs show the data points and the average of at least three biological replicates, relative to the WT strain at 6 h PS, and error bars indicate one standard deviation. Asterisks indicate a difference ($p < 0.05$ in Student's two-tailed *t*-tests) from the WT strain at the corresponding time PS and the asterisk above the bracket indicates a difference between the mutants.

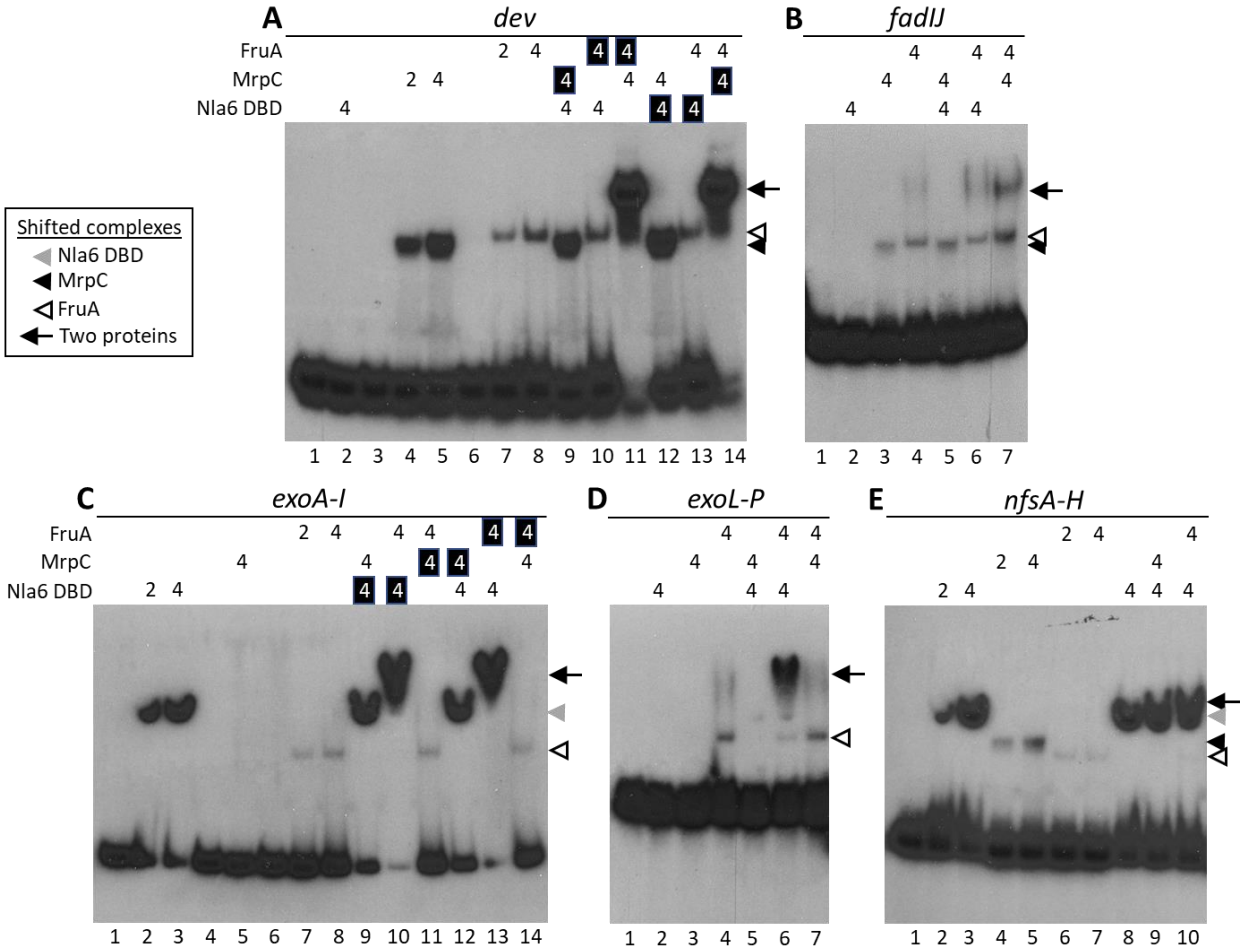

Figure 9. Binding of the Nla6 DBD, MrpC, and FruA to the promoter regions of the late-acting operons. EMSAs were performed with ^{32}P-labeled DNA fragments (2 nM) of the *dev* (-114 to -19) (A), *fadIJ* (-214 to -5) (B), *exoA-I* (-171 to -1) (C), *exoL-P* (-217 to +56) (D), and *nfsA-H* (-166 to +35) (E) promoter regions, and MBP-Nla6 DBD, His$_6$-MrpC, and FruA-His$_6$ at the μM concentrations indicated by numbers above each autoradiographic image. A white number on a black background indicates a protein that was added to the DNA-binding reaction 10 min later than the other protein. The positions of migration of shifted complexes are indicated along the side of each image by arrowheads for binding of individual proteins and by arrows for binding of two proteins (see boxed key). Lanes are numbered below images.

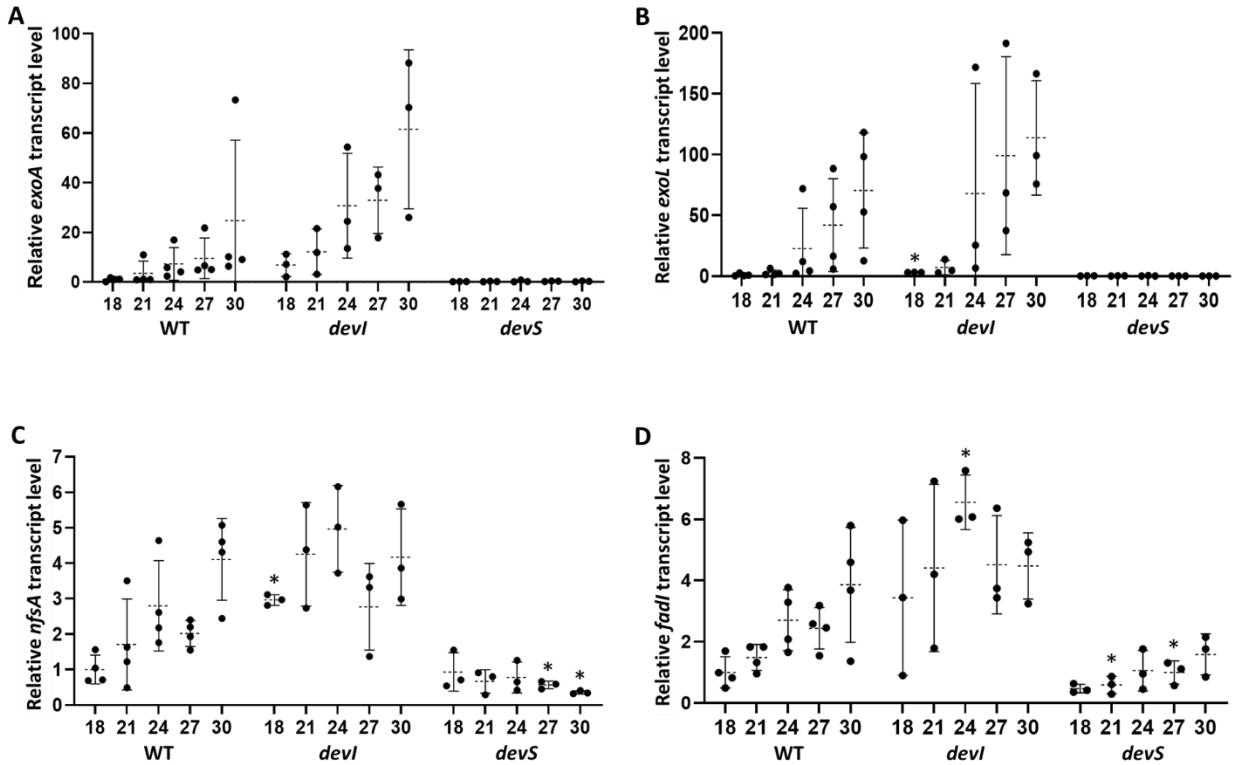

Figure 10. Transcript levels in *devI* and *devS* mutants during *M. xanthus* development. The WT strain and its mutant derivatives were subjected to starvation under submerged culture conditions. Samples were collected at the indicated times PS for measurement of *exoA* (A), *exoL* (B), *nfsA* (C), and *fadI* (D) transcript levels by RT-qPCR. Graphs show the data points and the average of at least three biological replicates, relative to the WT strain at 18 h PS, and error bars indicate one standard deviation. Asterisks indicate a significant difference ($p < 0.05$ in Student's two-tailed *t*-tests) from the WT strain at the corresponding time PS.

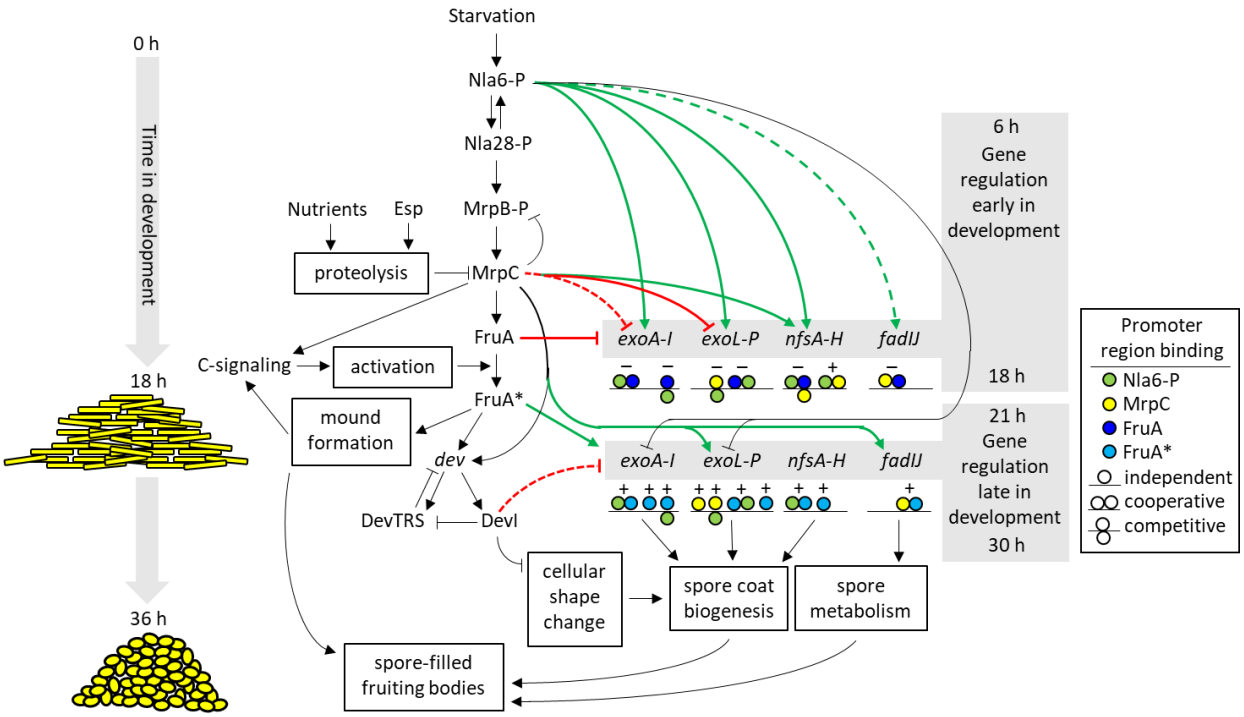

Figure 11. Model for regulation of late-acting operons during *M. xanthus* development. See the Figure 1 legend for explanation of the parts of the GRN that were known prior to this study. The new findings of our study are shown in color and are explained in the text. Briefly, the cartoon at left depicts a timeline of the developmental process with mounds forming by 18 h PS and spore-filled fruiting bodies forming by 36 h. Green arrows indicate positive regulation and red lines with a barred end indicate negative regulation. Solid arrows/lines indicate direct regulation and dashed arrows/lines indicate indirect regulation. Cartoons below the operons illustrate how independent, cooperative, and competitive binding of transcription factors to the promoter regions (see boxed key) could explain negative regulation early in development and positive regulation late in development. These cartoons are further explained in the Supporting Information.